Savi, S., Schildgen, T., Tofelde, S., Wittmann, H., Scherler, D., Mey, J., Alonso, R. N., Strecker, M. R. (2016): Climatic controls on debris-flow activity and sediment aggradation: The Del Medio fan, NW Argentina. - *Journal of Geophysical Research*, *121*, 12, pp. 2424—2445.

DOI: http://doi.org/10.1002/2016JF003912

AGU PUBLICATIONS

JGR

Journal of Geophysical Research: Earth Surface

RESEARCH ARTICLE

10.1002/2016JF003912

Key Points:
- Present-day aggradation in the Del Medio fan occurs within a transition zone between subhumid to arid climatic conditions
- Sediment supply is dominantly from landslides and rockfalls and transported by debris flows toward the Del Medio fan
- Aggradation in the Del Medio fan may provide a modern analog for past conditions that led to periodic aggradation in the Humahuaca Basin

Supporting Information:
- Supporting Information S1

Correspondence to:
S. Savi,
Sara.Savi@geo.uni-potsdam.de

Citation:
Savi, S., T. F. Schildgen, S. Tofelde, H. Wittmann, D. Scherler, J. Mey, R. N. Alonso, and M. R. Strecker (2016), Climatic controls on debris-flow activity and sediment aggradation: The Del Medio fan, NW Argentina, *J. Geophys. Res. Earth Surf.*, *121*, 2424–2445, doi:10.1002/2016JF003912.

Received 6 APR 2016
Accepted 18 NOV 2016
Accepted article online 25 NOV 2016
Published online 20 DEC 2016

Climatic controls on debris-flow activity and sediment aggradation: The Del Medio fan, NW Argentina

Sara Savi[1], Taylor F. Schildgen[1,2], Stefanie Tofelde[1], Hella Wittmann[2], Dirk Scherler[2,3], Jürgen Mey[1], Ricardo N. Alonso[4], and Manfred R. Strecker[1]

[1]Institute of Earth and Environmental Science, University of Potsdam, Potsdam, Germany, [2]GFZ German Research Centre for Geosciences, Potsdam, Germany, [3]Institute of Geological Sciences, Freie Universität Berlin, Berlin, Germany, [4]Facultad de Ciencias Naturales-Geología, Universidad Nacional de Salta, Salta, Argentina

Abstract In the Central Andes, several studies on alluvial terraces and valley fills have linked sediment aggradation to periods of enhanced sediment supply. However, debate continues over whether tectonic or climatic factors are most important in triggering the enhanced supply. The Del Medio catchment in the Humahuaca Basin (Eastern Cordillera, NW Argentina) is located within a transition zone between subhumid and arid climates and hosts the only active debris-flow fan within this intermontane valley. By combining ^{10}Be analyses of boulder and sediment samples within the Del Medio catchment, with regional morphometric measurements of nearby catchments, we identify the surface processes responsible for aggradation in the Del Medio fan and their likely triggers. We find that the fan surface has been shaped by debris flows and channel avulsions during the last 400 years. Among potential tectonic, climatic, and autogenic factors that might influence deposition, our analyses point to a combination of several favorable factors that drive aggradation. These are in particular the impact of occasional abundant rainfall on steep slopes in rock types prone to failure, located in a region characterized by relatively low rainfall amounts and limited transport capacity. These characteristics are primarily associated with the climatic transition zone between the humid foreland and the arid orogen interior, which creates an imbalance between sediment supply and sediment transfer. The conditions and processes that drive aggradation in the Del Medio catchment today may provide a modern analog for the conditions and processes that drove aggradation in other nearby tributaries in the past.

1. Introduction

In the Central Andes, studies of intermontane valley fills, fluvial and alluvial terraces, and fans on both the western and eastern flanks of the orogen have linked past phases of sediment aggradation to periods of enhanced landsliding and hillslope sediment supply [*Trauth et al.*, 2000, 2003; *Steffen et al.*, 2009, 2010; *McPhillips et al.*, 2013; *Bekaddour et al.*, 2014; *Schildgen et al.*, 2016] rather than to changes in discharge or in the transport capacity of the main rivers [*Hilley and Strecker*, 2005]. However, debate continues over the principal mechanisms leading to aggradation. Tectonic processes (including increased uplift or earthquake frequency), climatic processes (such as enhanced rainfall associated with either the El Niño–Southern Oscillation or variations in solar insolation), and autogenic processes of temporary sediment storage/evacuation have all been invoked to explain the alternations between sediment aggradation and incision phases that have affected the Central Andes [*Robinson et al.*, 2005; *Steffen et al.*, 2009; *Bekaddour et al.*, 2014; *McPhillips et al.*, 2014; *Margirier et al.*, 2015; *Schildgen et al.*, 2016].

In the northern sector of the Humahuaca intermontane basin in the southern Central Andes (Eastern Cordillera, NW Argentina), alluvial fill-terraces and fan deposits stand 150 to 200 m above the modern trunk-stream level (Figure 1a), testifying to past sediment supply and transport conditions that differ from those of today. Aggradation phases in this area, which today receives less than 200 mm of rainfall per year [*Bookhagen and Strecker*, 2008], have been dated to between ~800 and 40 ka B.P. [*Tschilinguirian and Pereyra*, 2001; *Robinson et al.*, 2005; *Strecker et al.*, 2007; *Schildgen et al.*, 2016] and have been linked to periods of increasing precipitation with an increased frequency of landslides and debris flows [*Tschilinguirian and Pereyra*, 2001; *May and Soler*, 2010; *Schildgen et al.*, 2016]. Although these previous studies argued against tectonic controls on past aggradation, no explanations have been offered to explain the location of sediment aggradation with respect to climate-related surface processes, and no attempts have been made to use modern aggradation patterns for providing insights into sediment dynamics in the Humahuaca Basin.

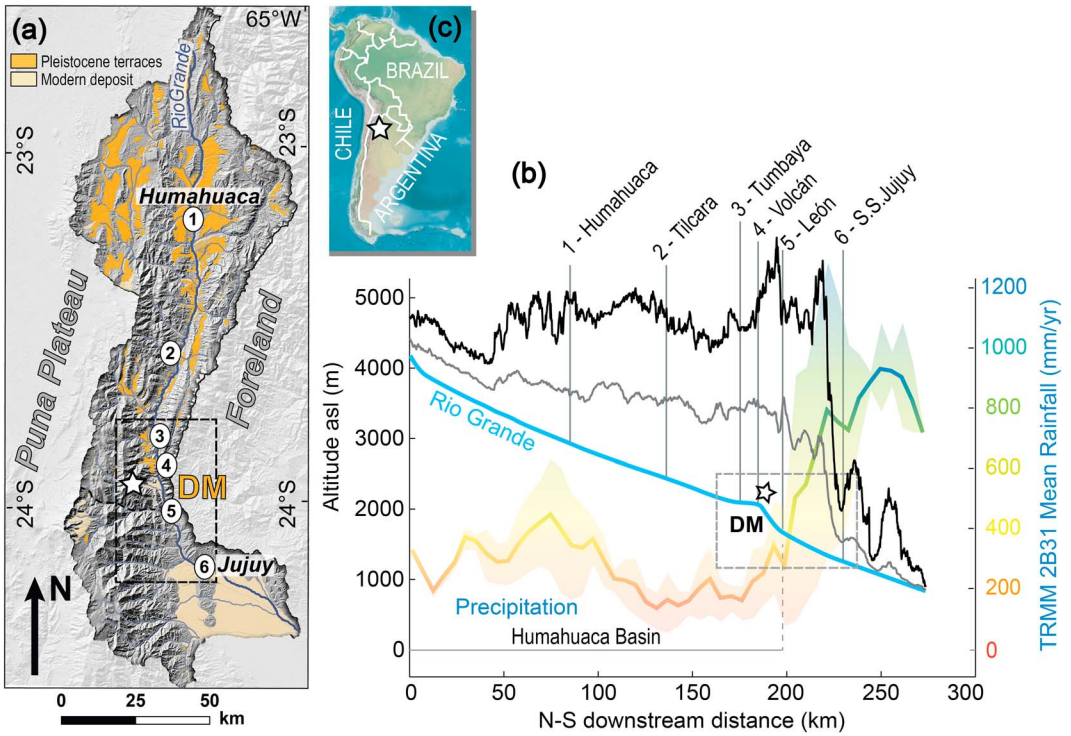

Figure 1. (a) Overview of the Humahuaca Basin. The orange overlay represents Pleistocene alluvial and fluvial terraces, whereas the light beige color represents the modern alluvial/fluvial deposits. (b) North-south swath profile of topography (the black and gray lines represent maximum and mean elevations) and precipitation (from blue to red; derived from calibrated satellite data of the Tropical Rainfall Measuring Mission (TRMM2B31)) [*Bookhagen and Strecker*, 2008] along the Río Grande. The large knickpoint along the Río Grande corresponds to the location of the Del Medio fan and to a climatic divide between arid conditions to the north and subhumid conditions to the south. This location is indicated by DM (Del Medio) and the star symbol. To ease orientation in the basin numbers identify villages along the Río Grande shown in Figure 1b. (c) Location of the Humahuaca Basin in NW Argentina. In Figures 1a and 1b the dashed rectangle shows the location of Figure 3.

At the southern end of the Humahuaca Basin, south of the village of Volcán (Figure 1), the ~60 km^2 Del Medio tributary catchment hosts the only extensive, active debris-flow fan in the area, which represents an important source of sediment for the Río Grande, the main alluvial river draining the Humahuaca Basin. The geometric and stratigraphic similarities between this fan and the late Pleistocene terraces and fans in the Humahuaca Basin farther north (e.g., the areal extent of the deposits and their thickness, grain size, sorting, and matrix) prompt an interesting question: Why is the Del Medio fan the only actively aggrading fan in the Humahuaca Basin today, when in the past, aggradation was much more widespread? Answering this question could help clarify the principal mechanisms that not only control aggradation in the Del Medio catchment today but may have also controlled aggradation episodes to the north in the past. To address this question, we first investigate what controls deposition in the Del Medio catchment, and why it is the only catchment within the Humahuaca Basin to maintain an actively aggrading fan. Second, we explore whether the same processes could have been responsible for the aggradation of valley fills during the Pleistocene.

To characterize the processes and local conditions that have led to aggradation in the Del Medio catchment, we combine field observations with measurements of in situ produced cosmogenic ^{10}Be in sand and pebbles. Differences in cosmogenic nuclide concentrations between sand and pebbles are thought to be related to the dominant erosional mechanisms [*Belmont et al.*, 2007; *Aguilar et al.*, 2014; *Codilean et al.*, 2008, 2014; *Carretier et al.*, 2015, and references therein; *Schildgen et al.*, 2016], with landslides releasing larger grains with lower ^{10}Be concentrations. In an effort to establish a chronology of the most recent activity on the fan, we determine exposure ages by measuring ^{10}Be concentrations of boulder surfaces and depth profiles. To examine why the Del Medio catchment is the only catchment that supports an active debris-flow fan, we also explore what possible factors related to topography, climate variability, lithology, and tectonics might focus

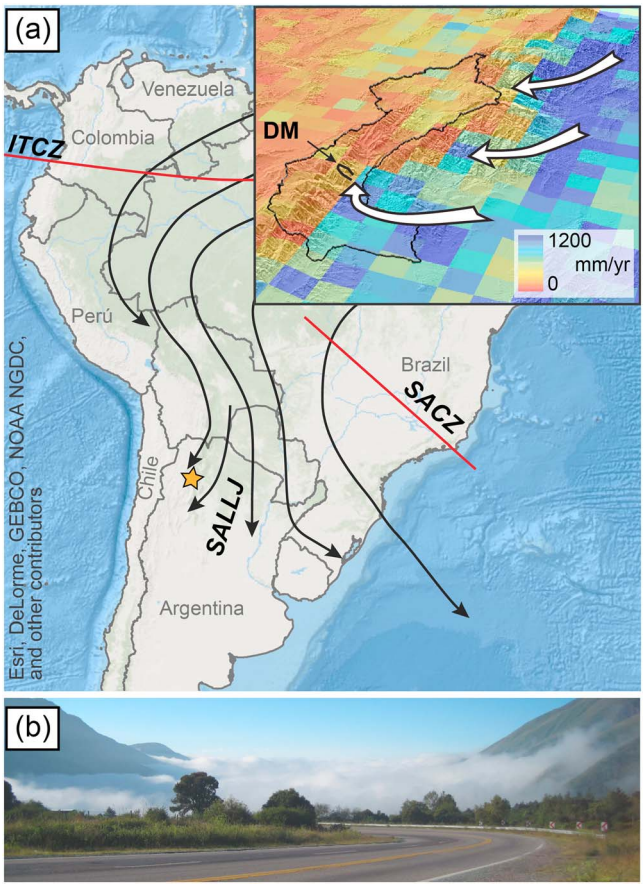

Figure 2. (a) Wind circulation systems affecting South America at ~850 hPa (modified from *Silva and Kousky* [2012], *Marengo et al.* [2004], *Vera et al.* [2006], and *Boers and Rheinwalt* [2014]). ITCZ = Intertropical Convergence Zone; SACZ = South Atlantic Convergence Zone; SALLJ = South America Low Level Jet; the star indicates the location of the study site. In the inset, annual rainfall distribution from TRMM satellite data (2B31) in the Humahuaca Basin (from *Bookhagen and Strecker* [2008]) with a sketch of wind vectors blocked by the orographic barrier plus the occasional northward penetration of humid air masses from the south. DM = Del Medio. (b) Looking south from the Del Medio fan: Clouds approaching; northward penetration of moisture from the southern margin of the Humahuaca valley (photo taken by S. Savi in 2014).

aggradation in this catchment. Finally, we discuss our results and observations in light of the age and location of the Pleistocene terraces farther upstream.

2. Study Site

2.1. Humahuaca Basin: Tectonic, Climatic, and Geomorphic Setting

The rock types exposed in the Humahuaca Basin comprise late Proterozoic metasedimentary rocks, early Paleozoic quartzitic sandstones, Paleozoic to Miocene intrusive rocks [*Jezek et al.*, 1985], and late Cenozoic sedimentary sequences [*González et al.*, 2000] (Servicio Geológico Minero Argentino (SEGEMAR) that document the transition from an unrestricted foreland basin to the present-day intermontane basin [*Pingel et al.*, 2013]. The eastern border of the basin was initially uplifted between 6 and 4.2 Ma following the eastward propagation of deformation within the Eastern Cordillera [*Pingel et al.*, 2013, 2014].

Today, the climate in the Eastern Cordillera is influenced by the South American Low-Level Jet (SALLJ) and the Chaco Low-Level Jet (CLLJ) during the austral summer, which bring moist air masses from the Amazon basin poleward along the eastern flanks of the Andes [*Salio et al.*, 2002; *Marengo et al.*, 2004; *Vera et al.*, 2006; *Boers et al.*, 2013]. In addition, the air masses associated with the South Atlantic Convergence Zone (SACZ) transport moist from the Atlantic toward the Andes [*Barros et al.*, 2000; *Mechoso et al.*, 2005; *Vera et al.*, 2006] (Figure 2). The Eastern Cordillera constitutes a barrier to these easterly air masses, creating a sharp east-west gradient in precipitation [*Bookhagen and Strecker*, 2008]. The Humahuaca Basin, however, is more prominently characterized by a N-S rainfall gradient that reflects the occasional northward penetration of moist air masses through the low-relief topography at the basin's southern outlet (Figures 2 and S3 in the supporting information). Rainfall decreases sharply from more than 800 mm yr^{-1} in the subhumid southern part of the basin south of the Del Medio fan to less than 200 mm yr^{-1} in the arid sectors north of the fan [*Castro*, 2001; *Bookhagen and Strecker*, 2008; *Marcato et al.*, 2009]. This rainfall pattern is mimicked by the vegetation pattern (Figure 3c).

Despite broad similarities in the structural setting and geology throughout the Humahuaca Basin (Figure 3a), the landscape exhibits important geomorphic differences north and south of the Del Medio fan (Figure 3b). In particular, the tributary catchments in the arid sector north of Volcán host thick fluvial fill terraces and fans (abandoned surfaces standing up to 150 m above the modern river level), while catchments in the subhumid sector south of the Del Medio fan record only limited deposition in the vicinity of the confluence with the Rio Grande. Landslides are known to occur throughout the Humahuaca Basin, both north and south of the fan,

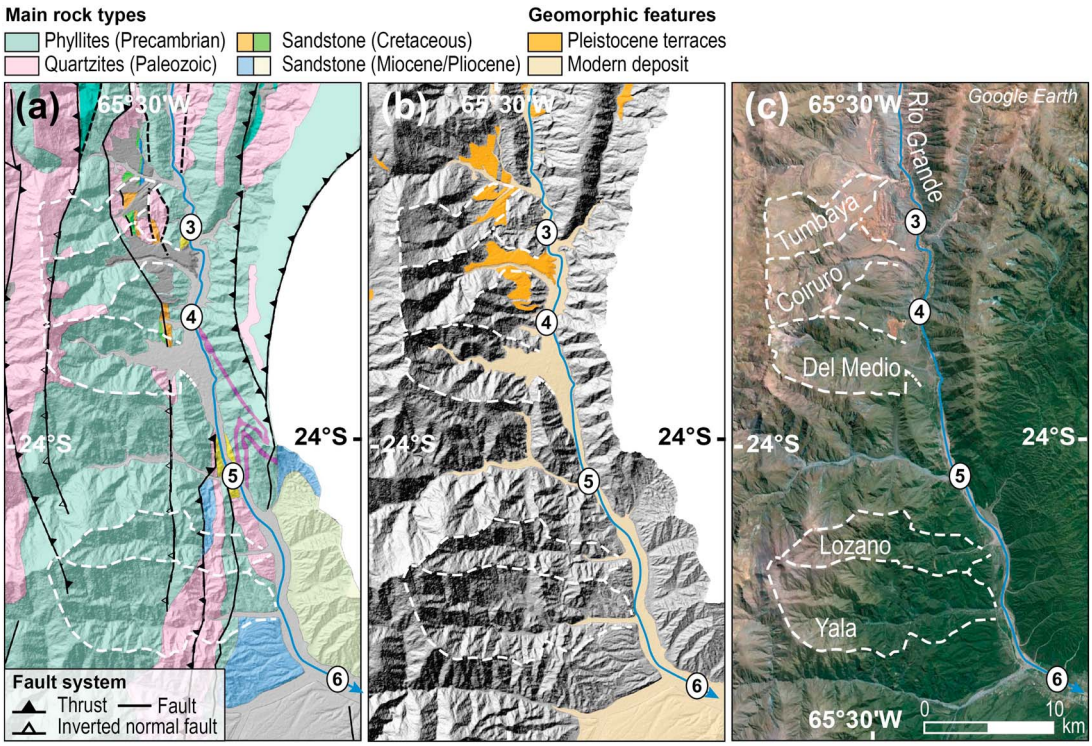

Figure 3. Area of the Humahuaca Basin spanning the climatic transition between subhumid and arid conditions. (a) Geologic and structural map of the area (modified from *Rodríguez Fernández et al*. [1999] and from the Geological and Mining Service of Argentina—SEGEMAR). (b) Late Pleistocene fill terraces and modern fluvial and alluvial deposition. (c) Google Earth map of the same area. Note the denser vegetation in the (greener) south, which reflects rainfall pattern (Figure S3). In all insets, we highlight (i) principal settlements (3 = Tumbaya; 4 = Volcán; 5 = León; 6 = San Salvador de Jujuy), (ii) the five catchments included in our morphometric analysis (including the Del Medio catchment, located south of the village of Volcán), and (iii) the southward-flowing Río Grande river.

with more frequent, low-volume landsliding events observed in wetter regions today [*Paolini et al*., 2005] and more frequent landsliding proposed to have occurred during wetter periods in the past across the region [*Trauth et al*., 2000; *Bookhagen et al*., 2001; *Haselton et al*., 2002; *Schildgen et al*., 2016].

2.2. The Del Medio Catchment

With ~18.6 km^2, the Del Medio fan occupies a substantial proportion of its ~58.8 km^2 catchment, especially when considering that at present, the steep source area of the fan covers an area of only ~16.7 km^2 at the western end of the catchment (Figure 4) [*Pastore and Groeber*, 1931; *Harrington*, 1946]. From the fan apex to where it connects with the Río Grande, the Arroyo Del Medio descends from 2970 m above sea level (asl) to 1965 m asl, with an average slope of ~10% (~5.75°). Today, the Arroyo Del Medio is the main active channel on the fan, although several abandoned channels and smaller active streams are visible on the surface. The incision of the Arroyo del Medio into the fan deposits reaches a maximum depth of ~25 m at the fan apex and decreases downstream. From surface observations and geometric calculations, *Pastore and Groeber* [1931] estimated a thickness of the alluvial deposits of ~50 m close to the fan apex and at least ~300 m at the channel outlet.

Steep slopes (up to 60° and 30° on average) characterize the source area of the Del Medio fan, with peaks along the western drainage divide exceeding 4 km in elevation (Figure 4). A prominent feature along the southeast-facing slope is the fresh scar of a rockfall/rockslide that occurred in 2009 (between the Cerro Peñorco and the Cerro Pabellón), whose deposits still occupy parts of the upper catchment. Several smaller landslide scars are visible throughout the catchment, but mostly within the NW sector (Figure 4). The main rock types include the intensely folded phyllites of the late Proterozoic *Puncoviscana Formation* and quartzites of the early Paleozoic *Mesón Group* [*González et al*., 2000] (Figures 3 and 4). Within the Del Medio catchment, there is no evidence of modern or past glacial activity [*González Díaz and Fauque*, 1987].

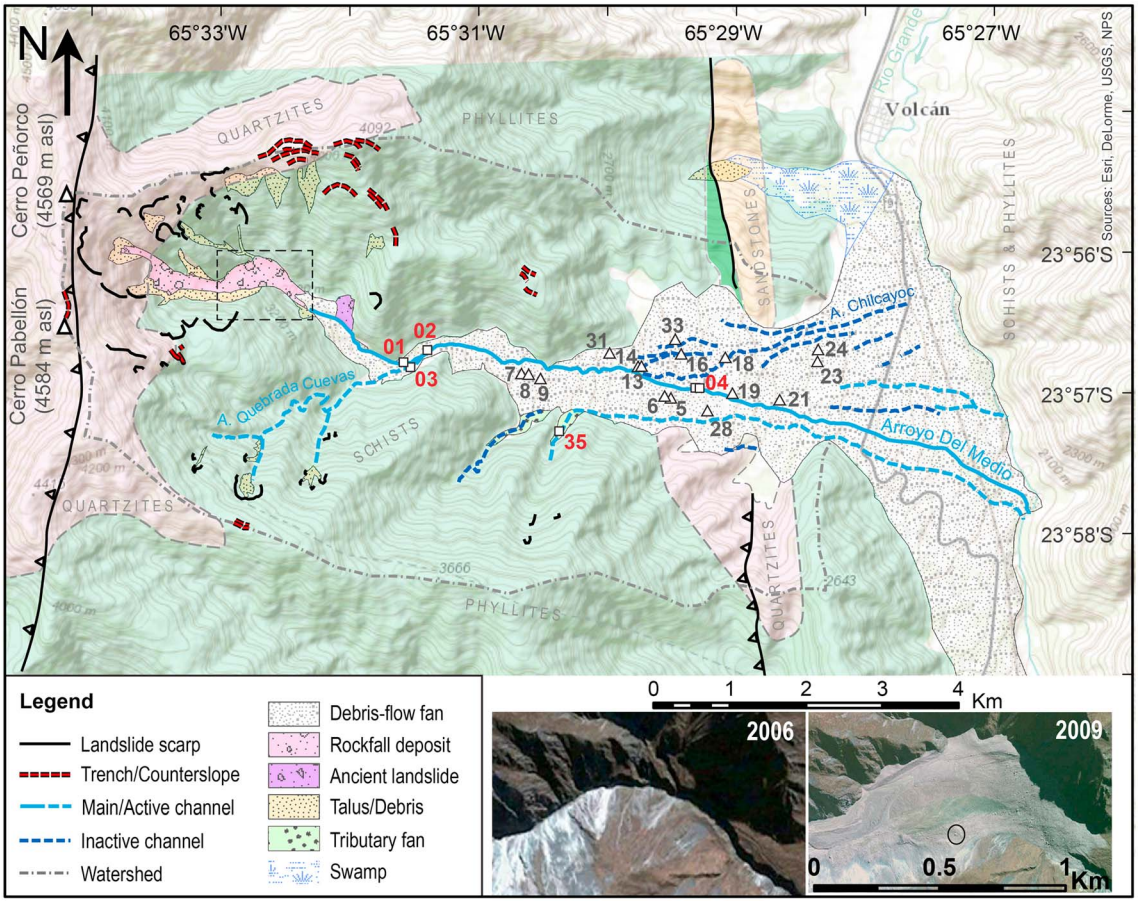

Figure 4. Geomorphic map of the Del Medio catchment and the location of the ^{10}Be samples. The white squares with red labels represent samples within the modern channel system. The white triangles with black labels represent sampled boulders. For simplicity and clarity of the figure, the prefix "ARDM" in the sample names has been removed (e.g., sample "ARDM02" is labeled "02" in the figure). The inset shows the upper catchment (area within the dashed square) before (2006) and after (2009) the rockfall event. In the small circle on the photo, a boulder with a diameter of 11 m is visible. Geologic units follow the legend in Figure 3.

The Del Medio fan appears to have formed a barrier to the Río Grande at times in the past: between the villages of Tumbaya and Volcán (upstream of the fan; Figure 1), the Río Grande meanders across lacustrine sediments on a subhorizontal surface [*Weigert et al*., 2010]; the sediments were deposited as a consequence of the repeated damming of the Río Grande from debris flows sourced in the Del Medio catchment [*Cencetti et al*., 2004; *Marcato et al*., 2009]. Approximately 3.5 km north of Volcán, the Río Grande incises into the lacustrine sediments; the incision continues downstream across the width of the Del Medio fan (~8 km wide in this location), exposing the fan stratigraphy to a depth of ~50 to 70 m. Downstream from the confluence with the Arroyo Del Medio, the Río Grande changes from meandering to a braided channel form while it drops ~400 m in elevation (~2070 m asl south of Volcán to ~1650 m asl at Léon: Figure 1b). Therefore, the Del Medio catchment marks the location of not only a change in the channel form of the Río Grande but also a modification of its longitudinal profile, which is gentle north of Volcán, but steepens rapidly downstream, thus defining a prominent knickpoint (Figure 1b).

2.3. Historical Debris Flows

Castro [2001] reconstructed the major debris-flow and flood events in the Humahuaca Basin based on newspaper reports and oral accounts. Consequently, only unusually large events that caused significant damage were recorded. The areas most affected are near the villages of Humahuaca, Tilcara, Maimará, Purmamarca, and Volcàn [*Castro*, 2001; Servicio Geológico Minero Argentino—http://sig.segemar.gov.ar/]. More than 70% of these events were registered between 1925 and 1945, with ~50% of the recorded activity affecting Volcàn [*Castro*, 2001].

In the Del Medio catchment, debris flows usually occur during the austral summer, when frequent and intense precipitation events can mobilize material in excess of 600,000 m^3 [*Cencetti et al*., 2004]. The first recognized activity on the Del Medio fan was reported by the traveler Acarette du Biscay in 1658 [*Acarette du Biscay*, 1663], who described mudflows affecting this area. The largest events were registered in 1928, 1941, 1945, 1984, and 1985 [*Castro*, 2001], but the area of the fan surface that was affected by these events is poorly known. Other studies reported events in 1923, 1930, 1943, 1954, 1972, 1987, 1988, 1989, 1990, and 2008 [*Pastore and Groeber*, 1931; *Harrington*, 1946; *Cencetti et al*., 2004; *Moreiras and Coronato*, 2010; *Weigert et al*., 2010; Servicio Geológico Minero Argentino—http://sig.segemar.gov.ar/]. The debris flow in 1945 is estimated to have been the most voluminous event in historical times [*Castro*, 2001]. It dammed the Río Grande, which subsequently formed a 2 km long lake that flooded the village of Volcán [*Castro*, 2001; *Cencetti et al*., 2004; *Weigert et al*., 2010]. The events in 1984/1985, with an estimated volume of 2.4×10^6 m^3, covered an important road (Ruta Nacional N°9) with more than 4 m of material over a distance of ~500 m [*Cencetti et al*., 2004; *Marcato et al*., 2009]. Because of the high frequency of debris-flow events, the railway that passed through the area was abandoned in 1992, and the Ruta Nacional N°9 was rerouted to a higher position less prone to damage [*Marcato et al*., 2009].

Whereas debris flows are probably the main mechanism of sediment transfer within the Del Medio catchment, landslides and rockfalls seem to be responsible for supplying sediment. *Harrington* [1946] described the situation in 1945, when a series of landslides and rockfalls provided the material for the subsequent debris flow that occurred later in the same year. The rockfall events in the source area persisted over several months [*Harrington*, 1946]. People living close to the fan during the event in 2009 also described a series of repeated landslides and rockfalls that occurred over the course of several months during the rainy season.

3. Materials and Methods

3.1. Geomorphic Mapping and Morphometric Features

To establish the area of the fan surface affected by debris-flow events and define our sampling strategy, we created a geomorphic map of the Del Medio fan based on interpretation of high-resolution satellite images (i.e., Google Earth, 2009) and field work during 2013. The image interpretation allowed us to map inaccessible areas and define individual deposits and geometries, whereas the field work allowed us to verify the extent of the deposits previously mapped and construct a relative chronology of the different debris-flow events based on geometric, cross-cutting, and topographic relationships.

To identify factors responsible for the Del Medio catchment's unique morphodynamics within the Humahuaca Basin, we performed a morphometric analysis of the landscape for five catchments (from south to north: Yala, Lozano, Del Medio, Coiruro, and Tumbaya) that span the transition from subhumid to arid conditions (Figures 3 and S3). We derived topographic metrics from an Advanced Spaceborne Thermal Emission and Reflection Radiometer Global Digital Elevation Model (a product of Ministry of Economy, Trade, and Industry and NASA) with a resolution of 30 m using ArcGIS and MATLAB software, including TopoToolbox v2 [*Schwanghart and Scherler*, 2014]. For the different catchments, we compared rock types, slope, local relief (calculated with a 500 m radius moving window), mean annual rainfall, and topographic roughness, defined as the topographic position index (TPI) [*Weiss*, 2001]. The latter parameter provides a reference topographic position for each cell of the digital elevation model in comparison with the average elevation of its neighboring cells, thus highlighting morphological features such as canyons, plains, and ridges. Additionally, we extracted the channel profiles, and the steepness (k_s) and concavity (θ) indices according to *Whipple* [2004].

3.2. Grain Size Dependency, Sampling Strategy, and Sediment Mixing

We measured ^{10}Be concentrations in sand and amalgamated pebble samples (maximum diameter of 4 cm) to analyze the processes responsible for sediment supply and transfer in the catchment. Where landslides appear to be less important in the catchment, we used the ^{10}Be concentrations to constrain denudation rates. In light of the frequent mass-wasting processes in the catchment, we expect the amount of ^{10}Be accumulated in most channels to be biased and not representative of a basin-average denudation rate [*Niemi et al*., 2005; *Yanites et al*., 2009]. However, ^{10}Be concentrations in active-channel sediment and fan deposits can still help to define the processes that govern the sediment routing system of the basin, specifically with respect to the importance of landslides and debris flows. We collected samples for ^{10}Be analyses from active channels at

three locations along the Arroyo Del Medio, at ~1.8, 2.0, and 5.8 km from the fan apex, and from two tributaries (Figure 3). The sample taken at 2.0 km from the fan apex (sample ARDM02) is located ~12 m downstream from the confluence of the Arroyo Del Medio with the Arroyo de la Quebrada Cuevas, allowing us to observe spatial variations of the ^{10}Be concentrations and to determine the degree of sediment mixing within the main channel (more detailed discussion can be found in the Text S2 in the supporting information [e.g., *Bierman and Steig*, 1996; *Granger et al*., 1996; *Binnie et al*., 2006; *Kober et al*., 2012; *Savi et al*., 2014, and references therein]). In all locations, we collected a sand sample of ~3 kg and a sample of 50–60 amalgamated pebbles from the active channel bed.

3.3. Exposure Ages of Boulders and the Fan Surface

We measured the concentration of in situ produced cosmogenic ^{10}Be in the surfaces of large boulders and in pebble samples from depth profiles for surface-exposure dating. We sampled 16 boulders deposited on the fan surface with diameters of 1.5 to 5 m and a height of 0.5 to 1.8 m, following the criteria of *Ivy-Ochs and Kober* [2008]. Large boulders are fairly uniformly distributed on the fan surface; however, due to the influence of human activity on the lower part of the fan, we focused our sampling on the middle section. On all boulders, we sampled the uppermost 5 cm of noneroded, regular, flat surfaces with a hammer and chisel (lack of erosion was established by field observations, including the absence of weathering and weathering-resistant quartz veins). The topographic shielding of incoming cosmic rays was estimated to be ~3% from field measurements of the surrounding topography. The sampled boulders were mainly derived from the quartzitic *Mesón Group*.

To estimate the fan-surface age and to define the most recent aggradation period within the exposed fan sediments, we used the depth-profile sampling approach proposed by *Anderson et al*. [1996]. Because ^{10}Be concentrations decrease with depth beneath a surface [*Lal*, 1991], an exponential fit through the plotted sample concentrations will yield an estimate of the ^{10}Be inheritance concentration of the sedimentary unit and the exposure age of the surface [e.g., *Siame et al*., 2004; *Braucher et al*., 2009]. For this purpose, we collected nine samples of the fan deposit along a 13 m depth profile exposed due to recent incision of the Arroyo Del Medio. All of the samples consist of 50 to 60 amalgamated pebbles with a maximum diameter of 4 cm (Figure S5). The samples were collected in horizontal layers of decimeter-scale thickness (Table 1) over a horizontal distance of 1 to 2 m. We used the Monte Carlo simulator of *Hidy et al*. [2010] to estimate the fan-surface age and the inherited nuclide concentration. As input parameters for the simulations, we used a mean altitude of 2400 m, a shielding factor of 0.946, a density range of 1.6 to 2.2 g cm^{-3}, a maximum erosion rate of 1 cm ka^{-1} with a total erosion threshold of 100 cm, and an attenuation length of 160 ± 5 g cm^{-2} (muogenic production is also included in the model of *Hidy et al*. [2010] and provides a ^{10}Be production rate of 0.140 atoms g^{-1} yr^{-1} and 0.246 atoms g^{-1} yr^{-1} for fast and negative muons, respectively). For the statistical calculation, we report results at a confidence level of 1σ with stochastic uniform errors. For the second (lower, buried) unit, we modified the simulation by using a chi-square confidence level (which allows a fit for more scattered data) with stochastic uniform errors and a constant attenuation length of 160 g cm^{-2}; we imposed the same maximum erosion rate of 1 cm ka^{-1} with a total erosion threshold of 100 cm.

3.4. Cosmogenic Nuclide Sample Preparation, Data Analysis, and Calculations

We followed standard procedures in our ^{10}Be sample preparation [*Kohl and Nishiizumi*, 1992; *von Blanckenburg*, 2004]. At the University of Potsdam, boulders and bedrock samples were crushed and sieved to obtain a grain size between 0.25 and 0.71 mm. Following the concentration of quartz grains through magnetic separation, the samples were treated with a series of acids, including HCl, HF, and HNO_3 to obtain purified quartz and remove meteoric ^{10}Be. The following steps were performed at the GeoForschungsZentrum (GFZ) Potsdam (Germany). Approximately 150 μg of ^{9}Be carrier was added to each sample, determined to have an average ^{10}Be/^{9}Be ratio of $0.60 \pm 0.26 \times 10^{-15}$ from several procedural blanks (see below). Quartz digestion was followed by column chemistry to isolate Be. The ^{10}Be/^{9}Be ratios were measured in BeO targets by accelerator mass spectrometry (AMS) at the University of Cologne (Germany), which uses the KN01-6-2, KN01-5-3, and KN01-5-1 standards with nominal ^{10}Be/^{9}Be values of 5.35×10^{-13}, 6.32×10^{-12}, and 2.71×10^{-11}, respectively. Corrections followed the standard of *Nishiizumi et al*. [2007] with a ^{10}Be half-life of $1.36\ (\pm 0.07) \times 10^{6}$ years.

Table 1. Values for the Calculation of Denudation Rates ("c" After the Sample's Name Stays for "Clast") and Exposure Ages

	Sample Name	Lat	Long	Elevation[a] (m)	Shielding	Production Rate[b]	Production Rate[c]
Denudation Rates	ARDM-01	−23.9445	−65.5257	3615	0.94	33.23	33.94
	ARDM-01c	−23.9445	−65.5257	3615	0.94	33.23	33.94
	ARDM-02	−23.9431	−65.5231	3596	0.94	32.95	33.83
	ARDM-02c	−23.9431	−65.5231	3596	0.94	32.95	33.83
	ARDM-03	−23.9446	−65.5252	3668	0.96	34.82	34.86
	ARDM-03c	−23.9446	−65.5252	3668	0.96	34.82	34.86
	ARDM-04	−23.9482	−65.4888	3473	0.95	31.03	31.93
	ARDM-04c	−23.9482	−65.4888	3473	0.95	31.03	31.93
	ARDM-35	−23.9516	−65.5058	3071	0.96	25.32	25.61
	ARDM-35c	−23.9516	−65.5058	3071	0.96	25.32	25.61
							Depth (m)
Depth-Profile	ARDM-01pA	−23.9482	−65.4895	3473	0.94	30.88	0.50–0.80
	ARDM-01pB	−23.9482	−65.4895	3473	0.94	30.88	1.00–1.20
	ARDM-01pC	−23.9482	−65.4895	3473	0.94	30.88	1.50–1.80
	ARDM-01pD	−23.9482	−65.4895	3473	0.94	30.88	2.00–2.25
	ARDM-01pE	−23.9482	−65.4895	3473	0.94	30.88	2.50–2.80
	ARDM-01 pF	−23.9482	−65.4895	3473	0.94	30.88	5.00–6.00
	ARDM-01pG	−23.9482	−65.4895	3473	0.94	30.88	7.70–8.00
	ARDM-01pH	−23.9482	−65.4895	3473	0.94	30.88	9.50–10.0
	ARDM-01pI	−23.9482	−65.4895	3473	0.94	30.88	12.0–13.0
Boulders-Exposure Ages	ARDM-07	−23.9464	−65.5114	2621	0.97	19.74	
	ARDM-14	−23.9457	−65.4964	2473	0.97	18.07	
	ARDM-13	−23.9458	−65.4965	2474	0.97	18.09	
	ARDM-19	−23.9491	−65.4851	2347	0.97	16.75	
	ARDM-28	−23.9511	−65.4879	2377	0.97	17.06	
	ARDM-18	−23.9449	−65.4859	2350	0.97	16.78	
	ARDM-09	−23.947	−65.5090	2596	0.97	19.45	
	ARDM-08	−23.9465	−65.5105	2613	0.97	19.65	
	ARDM-06	−23.8482	−65.4935	2438	0.97	17.66	
	ARDM-05	−23.9495	−65.4927	2423	0.97	17.55	
	ARDM-23	−23.9455	−65.4743	2254	0.97	15.82	
	ARDM-24	−23.9443	−65.4743	2252	0.97	15.80	
	ARDM-33	−23.9428	−65.4918	2433	0.97	17.65	
	ARDM-31	−23.9441	−65.5002	2497	0.97	18.34	
	ARDM-16	−23.9445	−65.4913	2409	0.97	17.40	
	ARDM-21	−23.9499	−65.4793	2302	0.97	16.30	

[a]For denudation rates this represents the mean elevation of the subbasin used in Cronus Calculator.
[b]Muonic plus spallogenic component as given by Cronus Calculator.
[c]Muonic plus spallogenic component as given by *Scherler et al.* [2014].

Because of the low ^{10}Be concentrations in our samples, the blank correction has a pronounced effect on the final calculations. To analyze this effect, we calculate erosion rates and boulder ages by using three different approaches: (i) following a single blank subtraction (each batch of samples was corrected separately based on the value of the blank within the batch), (ii) using the average blank value for all the blanks processed with our samples ($0.60 \pm 0.26 \times 10^{-15}$), and (iii) using a long-term average laboratory blank value (based on 12 blanks measured between July and September 2014 at the GFZ laboratory, $0.88 \pm 0.33 \times 10^{-15}$) (Text S3). The limit of detection (LOD), calculated as 3 times the standard deviation of the averaged blanks plus the mean value of the blanks [*Analytical Methods Committee*, 1987; *Mocak et al.*, 1997], is 22.31×10^3 atoms for the measured values and 28.92×10^3 atoms for the long-term GFZ blank value. The results of the different blank corrections are reported in Text S3, whereas throughout the text, we refer to the results of the single blank correction, which yielded the lowest uncertainties (more precise values).

All our results are based on the time-dependent ^{10}Be production-rate scaling scheme of *Lal* [1991] and *Stone* [2000], as implemented in the CRONUS Online Calculator ver. 2.2 (Table 2) [*Balco et al.*, 2008]. The sea level /high-latitude (SLHL) reference production rate for the calculations is 4.49 ± 0.39 atoms g^{-1} yr^{-1}, and the applied standard is 07KNSTD. For denudation-rate calculations, the results are reported as both (1) the output of the CRONUS online calculator v2.2, where we used the mean elevation of the catchment and mean basin shielding value to calculate ^{10}Be production rates, and (2) the output of a pixel-based approach [*Scherler et al.*,

Table 2. ^{10}Be Concentrations, Denudation Rates, and Exposure Ages (Reported for *Lal/Stone* Scaling Scheme) Obtained With Single Blank Corrections[a]

	Sample Name	^{10}Be (atoms g^{-1})	Error		Sample name	Erosion Rate (mm yr^{-1}) or Exposure Age (yr B.P.)	Error
Modern River Samples—Denudation Rates	ARDM-01	1,460	245	Modern River Samples—Denudation Rates	ARDM-01	13.8	2.58
	ARDM-01c	*170*	*64*		*ARDM-01c*	*118*	*51.8*
	ARDM-02	42,590	1,514		ARDM-02	0.48	0.040
	ARDM-02c	30,305	1,123		ARDM-02c	0.68	0.056
	ARDM-03	34,040	1,193		ARDM-03	0.63	0.052
	ARDM-03c	53,780	1,839		ARDM-03c	0.406	0.033
	ARDM-04	10,700	523		ARDM-04	1.8	0.16
	ARDM-04c	7,270	362		ARDM-04c	2.6	0.23
	ARDM-35	80,480	2,628		ARDM-35	0.21	0.017
	ARDM-35c	215,100	6,673		ARDM-35c	0.08	0.007
Boulders-Exposure Ages	ARDM-07	2,590	203	Boulders-Exposure Ages	ARDM-07	150	17
	ARDM-14	2,150	405		ARDM-14	130	28
	ARDM-13	1,905	368		ARDM-13	120	25
	ARDM-19	*941*	*287*		*ARDM-19*	*63*	*20.*
	ARDM-28	3,350	480.		ARDM-28	220	37
	ARDM-18	*747*	*265*		*ARDM-18*	*50*	*18*
	ARDM-09	2,460	402		ARDM-09	140	26
	ARDM-08	1,707	371		ARDM-08	98	23
	ARDM-06	2,540	428		ARDM-06	160	30.
	ARDM-05	2,550	446		ARDM-05	160	32
	ARDM-23	857	127		ARDM-23	61	10.
	ARDM-24	975	151		ARDM-24	69	12
	ARDM-33	5,400	323		ARDM-33	340	36
	ARDM-31	2,030	218		ARDM-31	120	17
	ARDM-16	1,580	167		ARDM-16	102	14
	ARDM-21	719	106		ARDM-21	50	8
Depth-Profile	ARDM-01pA	1,520	177				
	ARDM-01pB	1,060	152				
	ARDM-01pC	696	139				
	ARDM-01pD	417	105				
	ARDM-01pE	440	93				
	ARDM-01 pF	1,650	186				
	ARDM-01pG	1,080	152				
	ARDM-01pH	440	94				
	ARDM-01pI	1,200	149				

[a]Values in light grey are below the corresponding LOD value.

2014], which calculates a ^{10}Be production rate for each pixel within the contributing catchment based on its elevation and shielding value and then computes the catchment-average production rate to calculate the denudation rate (Table S6 in the supporting information). A lower SLHL ^{10}Be reference production rate calibrated for the Andes has been proposed [*Blard et al*., 2013]. Although we have not applied this rate when calculating our results, this alternative value would increase our exposure ages and decrease our erosion rates by 10 to 15% but would not change the overall interpretation of our results.

4. Results

4.1. Mapping Fan-Surface Morphology and Deposits

Debris-flow channels, levees, and different debris-flow deposits are visible on satellite imagery and are well preserved in the middle section of the fan, which was the target area of our sampling (Figure 4). In contrast, in the lower section, due to human modification of the fan surface, these features have been obscured. Abandoned debris-flow channels in the field are defined by well-preserved debris-flow levees and channel morphologies (Figure 5b). Different debris-flow lobes are characterized by different topographic heights and are typically characterized by the accumulation of similar-sized boulders at the frontal part of the deposit (Figures 5c and 5d). Together, these features allowed us to define a relative chronology of depositional events, based on geometric, cross-cutting, and topographic relationships, and to assign the sampled boulders to different debris-flow units.

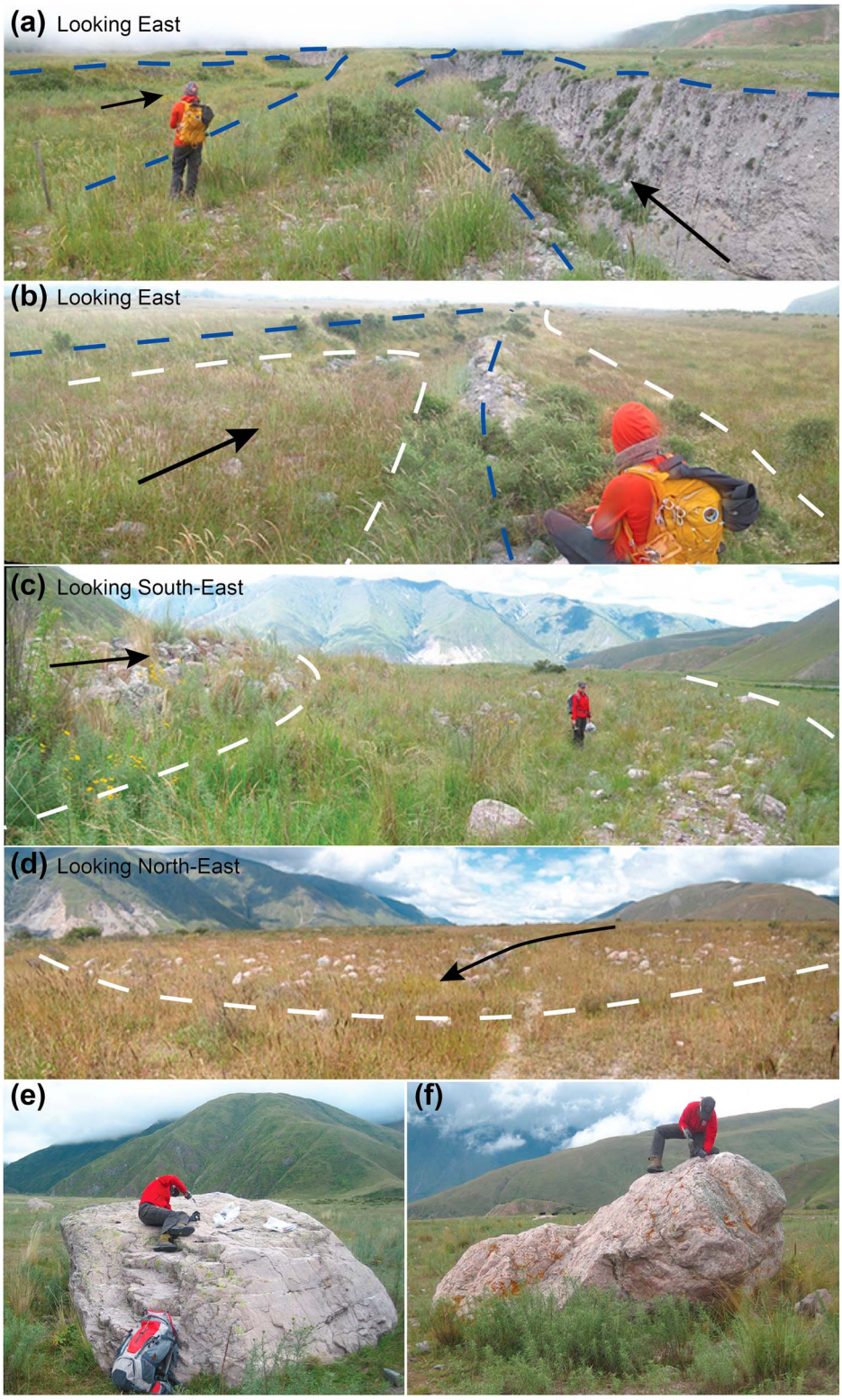

Figure 5. Photos from fieldwork: (a) the main Arroyo Del Medio (on the right) and the Arroyo Chilcayoc (on the left). (b) Inactive channel filled and blocked by a more recent flow. In the photos, the levees of the abandoned channel and the levee of the main Arroyo Del Medio (on the right side of the photo) can be seen. (c) Examples of debris-flow deposits on different topographic levels. (d) Lobe of a debris flow highlighted by boulders that are similar in size. In Figures 5a–5d, the black arrows indicate the flow direction; blue dashed lines represent levees or channels; white dashed lines represent deposits. (e and f) Examples of sampled boulders on the fan surface.

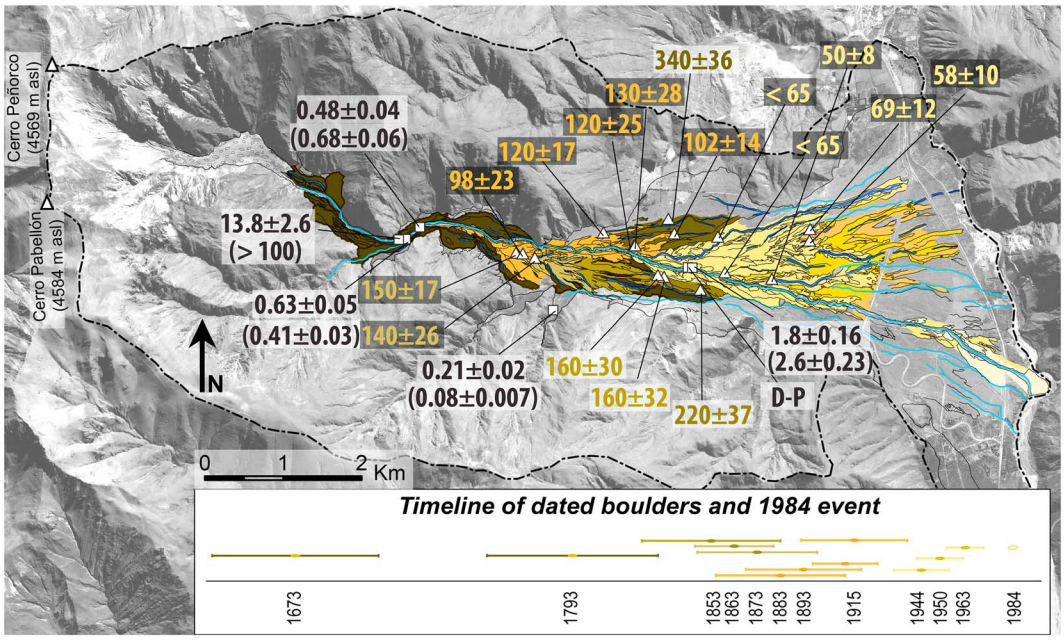

Figure 6. Map of debris-flow deposits together with the results of the modern denudation rates (white squares) from sand and pebbles (latter in parenthesis) and the dated boulders (white triangles). The denudation rates are in black (expressed in mm yr^{-1}), whereas the colored labels indicate the boulders ages in years B.P.. The label D-P indicates the location of the depth profile.

4.2. ^{10}Be Concentrations and Inferred Denudation Rates

Measured ^{10}Be concentrations in our river-sand and pebble samples vary by up to 3 orders of magnitude (Table 2 and Figures 6 and 7a). At the low end, pebbles collected from the main channel 1.8 km downstream from the fan apex (sample ARDM01) have a ^{10}Be concentration that is below the limit of detection (LOD). Thus, we can only constrain the denudation rate to be >100 mm yr^{-1} (see section 5.1 for further discussion). The associated sand sample has a ^{10}Be concentration of 1460 ± 245 atoms g^{-1} (1σ uncertainty), which yields a denudation rate of 13.8 ± 2.58 mm yr^{-1}. Samples ARDM02 and ARDM04, from the main channel at 2.0 and 5.8 km from the fan apex, have concentrations between $42{,}590 \pm 1514$ atoms g^{-1} (ARDM02) and 7270 ± 362 atoms g^{-1} (ARDM04c), yielding denudation rates of 0.48 ± 0.040 mm yr^{-1} and 1.8 ± 0.16 mm yr^{-1} for sand and 0.68 ± 0.056 mm yr^{-1} and 2.6 ± 0.23 mm yr^{-1} for pebbles. The two tributary samples, ARDM03 and ARDM35, have relatively high concentrations (between $215{,}100 \pm 6{,}673$ atoms g^{-1} and $34{,}040 \pm 1{,}193$ atoms g^{-1}), which yield denudation rates of 0.63 ± 0.052 mm yr^{-1} and 0.21 ± 0.017 mm yr^{-1} for sand and 0.41 ± 0.033 mm yr^{-1} and 0.08 ± 0.007 mm yr^{-1} for pebbles. As expected, our test of sediment mixing indicates poor or limited mixing within the main channel downstream of the two tributaries (Text S2).

4.3. Boulder-Exposure Ages

Most of the boulders we found on the fan surface were pink quartzites from the Cambrian *Mesón Group*, which confirms that the small area of the catchment, where the *Mesón Group* is cropping out (between the Cerro Peñorco and the Cerro Pabellón), is the main source area for the boulders. All dated boulders yield exposure ages of less than 400 years (Table 2 and Figures 6 and 7b). The oldest boulder (sample ARDM33: 340 ± 36 yr B.P.) is located in a lateral position, close to the northern edge of the fan. At the same longitude, but on the other side of the main channel, a few large boulders (Figures 5e and 5f) have ages between ~160 ± 30 and 220 ± 37 yr B.P.. Other boulders on both sides of the Arroyo Del Medio have ages of ~140 ± 24 yr B.P., 120 ± 21 yr B.P., 100 ± 18 yr B.P., and 60 ± 10 yr B.P.. Boulders ARDM18 and ARDM19 have a ^{10}Be concentration lower than the corresponding LOD, and therefore, they can only be considered as younger than 65 yr B.P.. Generally, the youngest boulders are found in the lower part of the fan, close to the channels of the Arroyo Del Medio and the Arroyo Chilcayoc, whereas the oldest boulders occupy laterally distal or higher topographic positions (Figure 6).

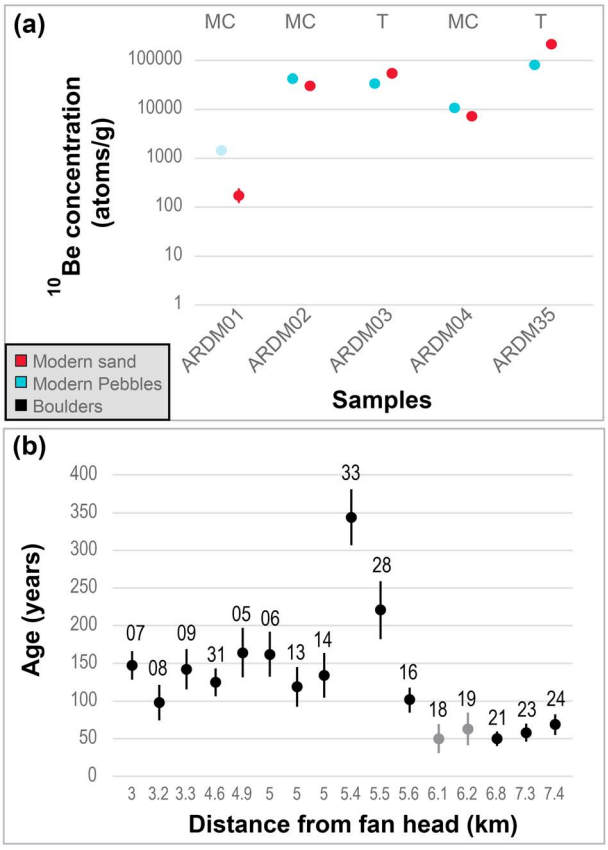

Figure 7. (a) Results of ^{10}Be concentrations of the modern river samples (note that ^{10}Be concentration values are shown on a logarithmic scale and the uncertainties are too small to be visible); MC = Main channel; T = Tributary. (b) Ages of the dated boulders versus downstream distance from the channel head of the Arroyo Del Medio (numbers at top of the columns are sample IDs). Samples are ordered as a function of distance using an uneven increment between points. Note that older samples are located close to the fan apex, whereas younger boulders are found in the more distal part of the fan. Oldest samples are located in the middle section of the fan in a lateral position (Figure 6). In Figures 7a and 7b, light colors indicate values below the Limit Of Detection (ARDM01-clasts, ARDM18, and ARDM19).

4.4. Depth Profile

The nine samples from the depth profile show what appear to be at least two decreasing exponential trends in ^{10}Be concentrations (Table 2 and Figure 8a): one represented by the upper five samples (from the surface to a depth of ~3 m) and a second one between ~5 and 9 m depth. The deepest sample at ~12 m below the surface (ARDM01pI) potentially represents the top of a third exponential trend. The sharp change in concentrations at ~5 m depth corresponds to a change in color of the exposed sediments, from light brown in the upper unit to dark brown in the lower unit.

Samples at the upper limits of these trends (ARDM01pA and ARDM01pF) have similar ^{10}Be concentrations of 1520 ± 177 atoms g^{-1} and 1650 ± 186 atoms g^{-1} (1200 ± 149 atoms g^{-1} for the deepest sample), whereas samples at the bottoms of the trends (ARDM01pE and ARDM01pH) have concentrations of 440 ± 93 atoms g^{-1} and 440 ± 94 atoms g^{-1} (Table 2 and Figure 8a). Because this pattern of ^{10}Be concentrations likely reflects two distinct fill units, we performed our Monte Carlo modeling separately for the upper five samples and for the three samples located between 5 and 9 m. The simulation results suggest an age for the surface of the fan (i.e., the upper unit) between 130 and 200 years (Figure 8b). After having corrected the ^{10}Be concentrations in the samples at depths of 5 to 9 m for postburial ^{10}Be production based on the age of the upper unit (following the approach of *Schaller et al*. [2002]), the model was run for the lower unit following two different scenarios: (1) sample ARDM01pF represents the surface of the lower unit or (2) sample ARDM01pF is 50 cm below the former surface of this unit (depth of the sample below the color change). These two scenarios were introduced due to the uncertainties related to the position of the paleo-fan surface and the lack of a distinct boundary between the two units in the field. The model results suggest ~70 years of exposure of the lower unit in the first scenario and between 110 and 130 years in the second one. Hence, the lower unit was deposited between 200 and 330 years ago, which is in agreement with the oldest ages obtained from the surface boulders. The model results also suggest mean and maximum inheritance values of 200 atoms g^{-1} and 300 atoms g^{-1} for the upper unit, and a mean and maximum inheritance of 500 atoms g^{-1} and 600 atoms g^{-1} for the lower unit.

4.5. Morphometric Parameters

Our morphometric analyses highlight differences and similarities among the tributary catchments spanning the N-S climatic gradient in the Humahuaca Basin (Figure 9). Overall, different rock types are similarly distributed within the catchments (Figures 4 and 9). In the Del Medio and Coiruro catchments, the slope maps

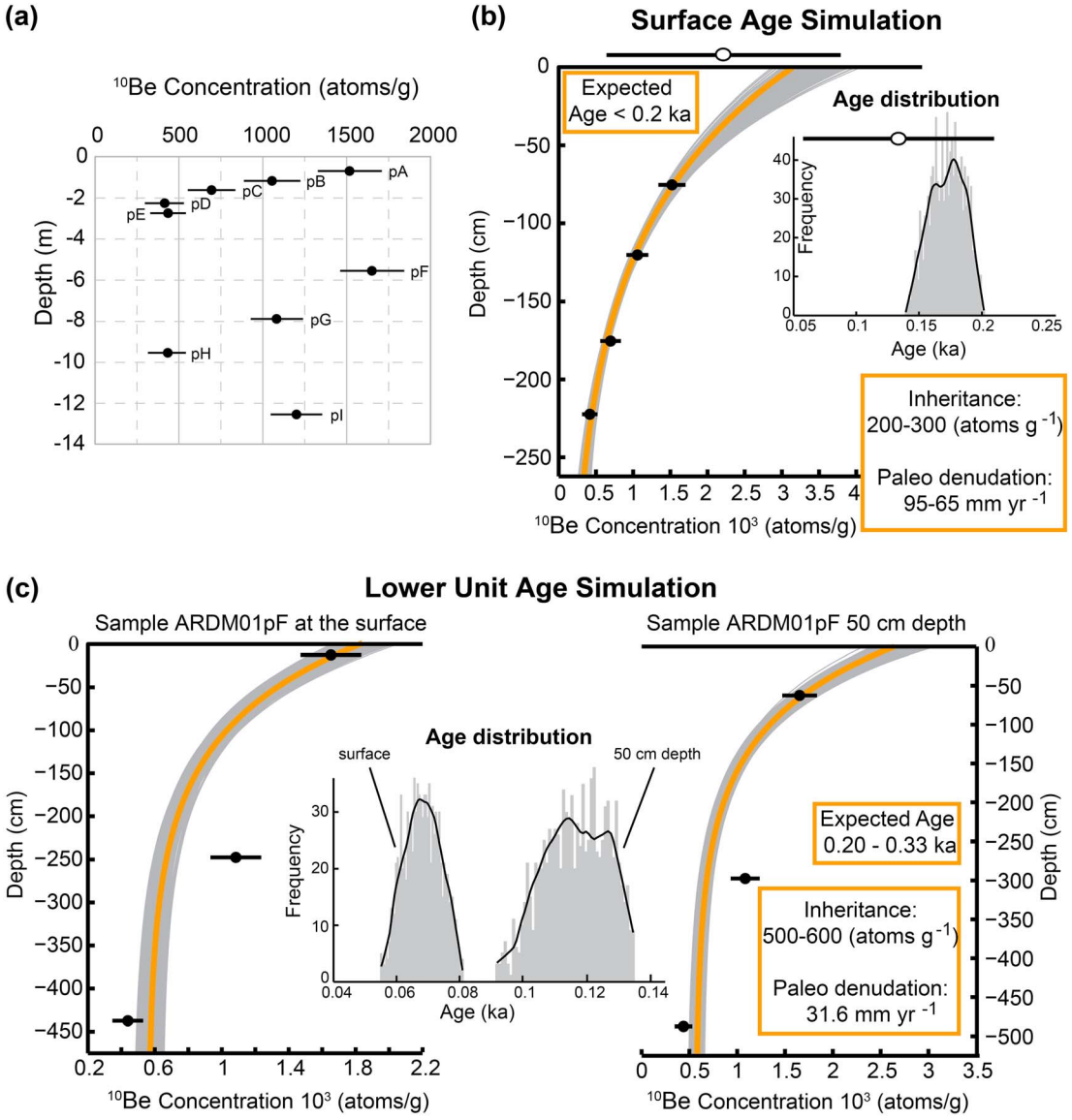

Figure 8. (a) The ^{10}Be concentrations of the depth profile. (b and c) Acceptable fits for upper and lower unit using the *Hidy et al.* [2010] Monte Carlo simulation. Simulation of the upper unit exposure age (Figure 8b). The white ellipse at the top of the graph represents the average concentration of the boulders dated on the surface of the fan ± 1 standard deviation. The simulation of the lower unit age suggests a most likely age exposure of ~70 years, when sample ARDM01pF is considered at the surface, and an exposure of 110–130 years when it is considered at 50 cm below the paleo-surface (Figure 8c).

reveal a slightly larger portion of steep slopes in the source areas compared to the others, but overall, the differences are small (less than 5 degrees). The only exception is the Tumbaya catchment, which is characterized by a landscape with gentle slopes in its headwaters, which is also well portrayed on the relief map. The relief maps further highlight the similarities between the Del Medio and Coiruro catchments, both of which are characterized by an extensive area of high relief in their upper parts. The low-relief area in the middle of the Yala catchment is the consequence of a landslide that impounded streams and formed several small lakes [*González Díaz and Mon*, 2000; *Lupo et al*., 2006].

The results of the topographic position index (TPI) analysis differ more substantially. In particular, the Yala and Lozano catchments are characterized by narrow and deep valleys, whereas valley width is slightly larger in the other basins. In all catchments, with the exception of Coiruro, the valleys are deeply incised in their upper parts, but have wide and gentle sloping valley floors farther downstream. The TPI also highlights the convex shape of the Del Medio fan, the Coiruro alluvial terrace, and the flat upper Tumbaya catchment.

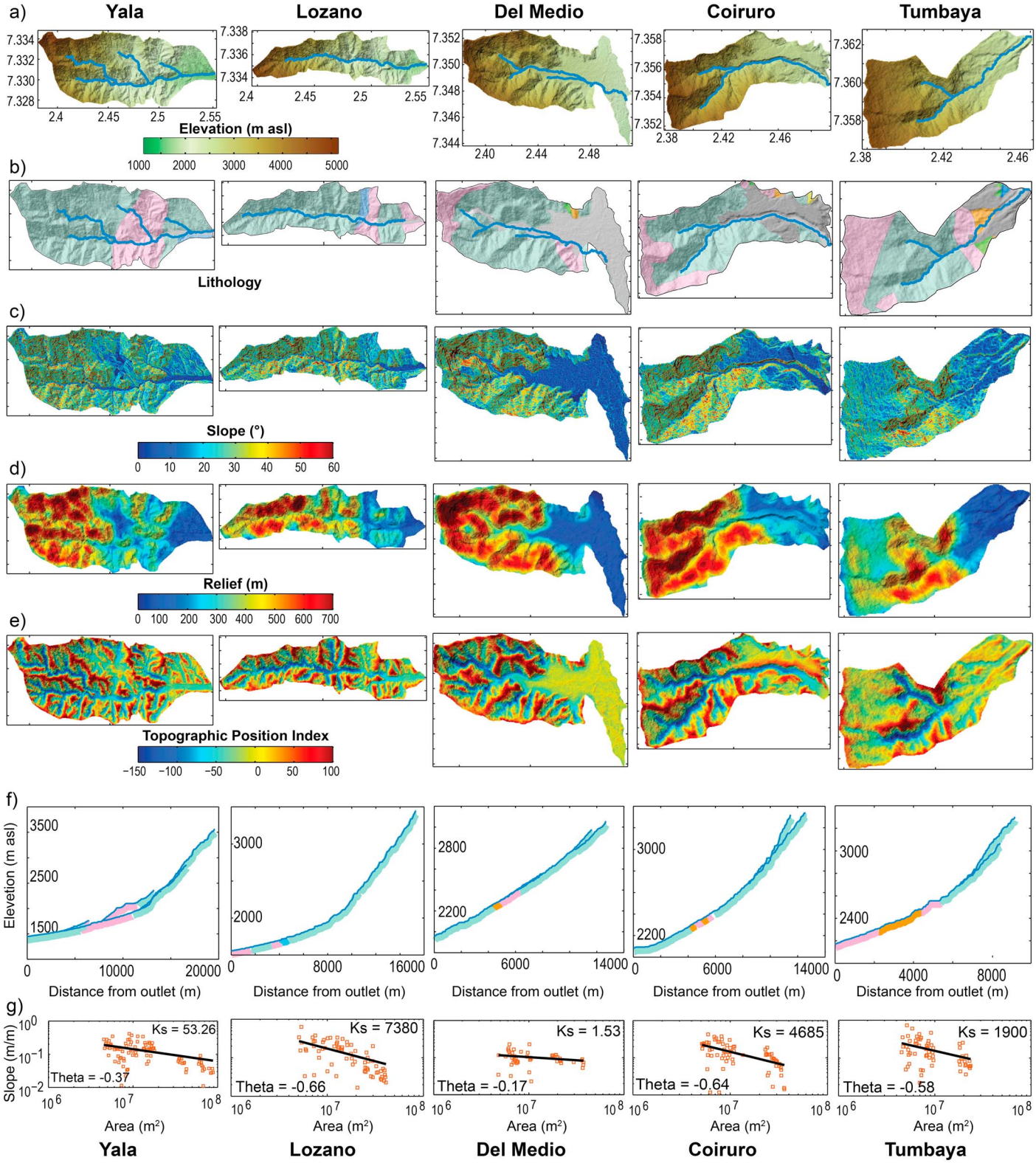

Figure 9. Geomorphic parameters of catchments spanning the N-S climatic gradient in the Humahuaca Basin. Catchments are ordered from (left) south to (right) north. Maps show the universal time meridian (UTM) coordinates of the catchments (UTM latitude × 10^6 m, UTM longitude × 10^5 m). (a) Elevation, (b) lithology, (c) slope, (d) relief, (e) topographic position index, (f) river profiles, and (g) slope versus area plots (Ks = steepness index; theta = concavity index). The legend for geologic units is as in Figure 3; rock types are also indicted by the colored bars beneath the river profiles. Changes in rock type do not seem to influence the morphology of the channels.

The river profiles also show clear differences, with a well-developed concave-upward shape for the Yala and Lozano channels, a slightly concave shape for the Coiruro and Tumbaya channels, and a relatively straight profile (very low concavity) for the Arroyo Del Medio. Changes in rock type do not seem to strongly affect the shape of the channels, as no knickpoints are seen at lithological boundaries. The low concavity of the Arroyo Del Medio is evident also from the slope-area plots, where the data define a subhorizontal line, which is typical of debris-flow dominated channels [e.g., *Montgomery and Foufoula-Georgiou*, 1994] (Figure S6).

5. Discussion

5.1. Surface Processes in the Del Medio Catchment

Low ^{10}Be concentrations in sediments that are typically found in areas affected by landslides are unlikely to represent basin-averaged denudation rates, as (1) these rates may be biased by inputs of low-concentration material sourced from large, stochastic mass-wasting events (particularly for small catchments), and (2) because large landslides may disrupt sediment mixing for prolonged periods [*Niemi et al*., 2005; *Yanites et al*., 2009; *Savi et al*., 2014] (see Text S2), violating a required key assumption when converting detrital ^{10}Be concentrations into basin-wide mean denudation rates [*von Blanckenburg*, 2005]. However, pebbles and larger clasts that indicate lower cosmogenic concentrations compared to sand have been commonly interpreted to reflect landslide activity within a river catchment [*Brown et al*., 1995; *Matmon et al*., 2003; *Belmont et al*., 2007; *McPhillips et al*., 2014; *Schildgen et al*., 2016], providing a useful indicator of both hillslope processes and potential bias in calculated denudation rates [*Lukens et al*., 2016]. Our data from the Del Medio catchment illustrate high variability of ^{10}Be concentrations, including some examples of strong grain-size dependence (Figures 7 and 8). In particular, the three samples taken from channels that drain the region impacted by the 2009 rockfall (ARDM01, ARDM02, and ARDM04) have higher ^{10}Be concentrations in sand compared to pebbles. The samples from the two tributaries (ARDM03 and ARDM35), in contrast, show lower ^{10}Be concentrations in sand samples compared to pebbles (Figure 7a). Although we mapped some small landslide scars in those tributaries, particularly in the tributary of sample ARDM03 (Figure 3), they apparently do not result in lower ^{10}Be concentrations in pebbles compared to sand, implying that these relatively small mass-wasting events do not lead to significant grain-size dependency. Observed differences in ^{10}Be concentrations throughout the study area may rather be related to lithologic differences and their propensity for landslides, as explained below.

5.1.1. Rock-Type Influence on Landslide Activity

The Arroyo Del Medio, which records the lowest ^{10}Be concentrations of all the channels in the Del Medio catchment, drains an area where mainly *Mesón Group* quartzites are exposed (Figure 3). Considering that the debris-flow boulders on the fan are primarily composed of quartzite, and that landslide scars are common along the boundary of the *Mesón Group* in the northwestern part of the catchment, the jointed rocks of the *Mesón Group* may be particularly prone to slope failures. The propensity to fail may also be high at the contact between the *Puncoviscana* phyllites and the *Mesón Group* quartzites, as observed in a similar setting in the Quebrada del Toro intermontane basin farther southwest [*Marrett and Strecker*, 2000]. The two tributaries of the Arroyo del Medio, in contrast, mainly drain the *Puncoviscana* phyllites. The higher ^{10}Be concentrations in both sand and pebbles for these tributaries imply that the *Puncoviscana* formation is mainly exhumed by soil creep or other shallow mass movements, rather than by deep-seated landslides. The virtual lack of landslide scars in the tributary catchments supports this interpretation (Figure 4). The slightly lower ^{10}Be concentration in a sample from a tributary farther west (ARDM03) is probably associated with steeper hillslopes and some minor landslide activity based on the presence of small landslide scars.

5.1.2. Contribution of Landslides to Sediment Flux

The amalgamated pebble sample collected closest to the modern landslide deposit (ARDM01), which we infer would be most indicative of a modern landslide signal, has a ^{10}Be concentration of 170 ± 64 atoms g^{-1}. This concentration is similar to the inherited concentrations we obtained from the upper depositional unit within the depth profile (between 200 and 300 atoms g^{-1}). The consistency between the concentrations is not surprising, because the sediment within the sampled deposit is only 200 years old and was likely associated with similar erosion and transport events that affect the drainage basin today. The inherited concentration derived from the lower depositional unit (between 500 and 600 atoms g^{-1} from sediment approximately 400 years old) is 2 to 3 times higher, but still represents an extremely low concentration that is unlikely to reflect different erosion and transport processes compared to the upper unit. Because the

inheritance-corrected exposure age of the fan surface derived from the depth profile overlaps with the exposure ages of the boulders, which are calculated assuming no inheritance, it is likely that inheritance in the boulders is indeed negligible, similar to observations from moraine deposits [i.e., *Heyman et al*., 2011]. Otherwise, we expect that the boulders would yield significantly older ages compared to the fan surface. Together, the extremely low inheritance values in both parts of the profile highlight the speed at which sediment is produced and deposited on the fan. As such, these data corroborate our inference that a combination of landsliding and debris-flow activity has dominated sediment production and transport in the Del Medio catchment, at least over the last several hundred years. The very low channel concavity of the Del Medio catchment revealed in the slope-area plots supports the dominance of landslide- and debris-flow processes over longer time scales (Figure S6).

5.2. Debris-Flow Activity Across the Fan Surface

Our boulder exposure ages (Figure 6) and depth-profile results (Figure 8) illustrate that almost the entire middle section of the fan has been affected by debris flows within the last few centuries. These results suggest that the sediment routing system in the Del Medio fan is highly dynamic, with frequent channel avulsions that spread sediment across the entire width of the middle sector of the fan. The downstream shift of the debris-flow activity toward lower areas of the fan between 100 and 70 years ago may be associated with incision of the Del Medio channel head [e.g., *Dühnforth et al*., 2010]. This incision could reflect a change in the climatic regime, or it could be related to internal dynamics of the catchment associated with re-filling and removal of material in the source area. The additional shift toward the lower part of the fan after the 1945 event (after which the Arroyo del Medio became the main channel) could have been related to either human activity [*Weigert et al*., 2010] or to a shortage of mobilized material when not enough material in a single debris flow is able to overtop the steep walls of the modern channel. This latter hypothesis could be particularly important for hazard assessments, especially in light of the recent large accumulation of material caused by the 2009 landslide, which could potentially feed future large debris flows and reactivate abandoned channels.

5.3. Tectonic, Lithologic, and Autogenic Influences on Fan Activity

In the Humahuaca Basin, the lack of any temporal coincidence between debris-flow events and earthquakes in the recent past (Text S1) argues against seismicity triggering debris flows in this area, in contrast to what has been inferred for the western central Andes [*Antinao and Gosse*, 2009; *McPhillips et al*., 2014]. Although there is evidence for Quaternary tectonic activity [*Pingel et al*., 2013, and references therein], currently, most of the faults in the Humahuaca Basin appear to be aseismic. Instrumentally recorded seismicity in the region of the Del Medio catchment occurs at depths greater than 150 km, which is associated with the subducting Nazca Plate, and results in small ground accelerations (data from the Northern California Earthquake Data Center, U.S. Geological Survey Earthquakes Hazards Program, and the Instituto Nacional de Prevención Sísmica of Argentina (Figure S1). It is unknown, however, if earlier earthquakes in the Humahuaca region had greater magnitudes or higher frequencies capable of triggering landslides. The tectonic deformation of Quaternary valley-fill deposits farther upstream attests to recent tectonic activity [*Pingel et al*., 2013], suggesting that past seismicity might have influenced the generation of mass movements whose deposits were subsequently remobilized as debris flows during extreme precipitation events. In this case, we need to explain why only the Del Medio catchment has been affected in recent times.

The location of the Del Medio fan, which corresponds to a large knickpoint in the river profile of the main Rio Grande, could be associated with a tectonic structure that might, in turn, affect sedimentation at the Del Medio fan. The effects of tectonic uplift on the threshold hillslopes of the Del Medio catchment could be responsible for the high frequency of landslides and high sediment supply in this particular location. However, our morphological analysis (Figure 9) shows that no significant morphological difference between the neighboring catchments is able to explain why the Del Medio catchment is the only one with an active debris-flow fan. Also, it is difficult to associate the knickpoint with an isolated local, active structure, considering that no bedrock is exposed in the channel of the Rio Grande anywhere within the Humahuaca Basin. Furthermore, the regional fault system has an east-verging, N-S to NNE-SSW orientation (Figure 3a) [*Rodríguez Fernández et al*., 1999; *Pingel et al*., 2013], implying that if a fault was to cross the river at the knickpoint, the upstream section should be uplifted faster than the downstream section. However, river steepness values are higher downstream from the knickpoint; hence, the mapped fault system is not compatible with

the observed knickpoint. In the alternative case of an upstream-migrating knickpoint, associated with a transient response to faster uplift of the whole region, one would expect to find knickpoints throughout the whole river network (i.e., along tributary valleys) [e.g., *Kirby and Whipple*, 2012], which is not the case. These observations argue against the steepening in the channel profile marking either a quasi-static knickpoint that might be associated with an active structure, or an upstream-migrating knickpoint associated with faster uplift of the whole region. More likely, the knickpoint represents a disruption to the main channel induced by a major, localized source of sediment.

Different rock types may have a variable propensity toward failure (either seismic or climatic triggers), as we argued in the previous section. However, mean catchment slope in the different basins' headwater areas differs by less than 5°, suggesting that differences in slope are not a primary cause for the degree of fan activity. Also, the rock types and faults in the Del Medio catchment are also present in neighboring catchments, which show no recent debris-flow activity. Although it remains possible that localized weakening preferentially affects erosion in the Del Medio catchment (if, for example, faults cut across the steep headwall of the catchment), this would not explain why the locus of aggradation has shifted over time, from farther up the valley during the Pleistocene to the Del Medio catchment today.

Finally, aggradation in the Del Medio catchment could also be driven by autogenic processes. However, considering the relatively small size of the catchment relative to the fan, and the rapidity of erosional and depositional processes that we observe, it is difficult to envision how this substantial sedimentary fill could be generated through a delayed or complex response within the catchment [e.g., *Schumm and Parker*, 1973; *Slingerland and Snow*, 1988]. Also, as pointed out by *Daniels* [2008], autogenic bed-elevation changes should be time-transgressive, but we find that nearly the whole exposed surface of the fan has an exposure age spanning only a few hundred years. Additionally, the absence of mobilized material in the source area before the 2009 landslide (inset of Figure 4) argues against a sustained sediment flux supplied by ancient landslides [i.e., *Scherler et al*., 2016]. Although shifts in the location of sediment deposition on the fan may be autogenic on relatively short time scales [e.g., *Coulthard et al*., 2002], we do not consider it plausible that the entire deposit was created through autogenic processes.

5.4. Climatic Influence on Fan Activity

Climatic conditions have been suggested to play a pivotal role in modulating both sediment supply from the hillslopes and transfer of sediment through channels within the various subcatchments of the Humahuaca Basin [*Schildgen et al*., 2016], a relationship that has been demonstrated in many other parts of the world as well [*Bull*, 1991; *Dethier and Reneau*, 1996; *Schildgen et al*., 2002; *Stock and Dietrich*, 2003, 2006; *Lavé and Burbank*, 2004; *Bookhagen et al*., 2005, 2006]. Ideally, one would relate sub-millennial scale climatic variability to the generation of cut-and-fill cycles to understand fan activity [*Bull*, 1991], but the temporal resolution of our data limits us to examining broad scale controls on aggradational phases and associated fan activity. For the Del Medio catchment, our field observations, ^{10}Be data, and morphometric analyses corroborate the hypothesis that rockfall and landslide events are the main processes of sediment supply, whereas debris flows are the main mechanisms for sediment transport. Satellite images and our morphometric analyses of catchments spanning the climatic gradient additionally indicate that pronounced sediment aggradation and frequent debris flows are particular to the Del Medio catchment. Because the Del Medio catchment is located within the transition between subhumid conditions to the south and arid conditions to the north, the source area of the fan occasionally receives higher amounts of precipitation compared to the northern catchments. Indeed, *Castino et al*. [2016] showed that the NW Argentine Andes are subjected to pronounced changes concerning the amount and the location of hydro-meteorological extreme events during episodes of enhanced climatic variability. In such a context it is conceivable that an increase in rainfall can increase pore pressures along the hillslopes that trigger landslides and potentially also trigger debris flows that transport sediment across the fan.

The imbalance between sediment supply and fluvial transport capacity within the Del Medio catchment ultimately causes fan aggradation. In contrast, more abundant rainfall and runoff in tributaries that are located south of the climatic divide (i.e., Yala and Lozano catchments) do not allow for significant sediment storage. The higher vegetation density of the two southern catchments (Figure 3c) may additionally help to stabilize hillslopes and reduce the amount of sediment supplied to the channel network [e.g., *Istanbulluoglu and Bras*, 2006; *Torres-Acosta et al*., 2015], potentially creating supply-limited conditions. In contrast, to the north of the

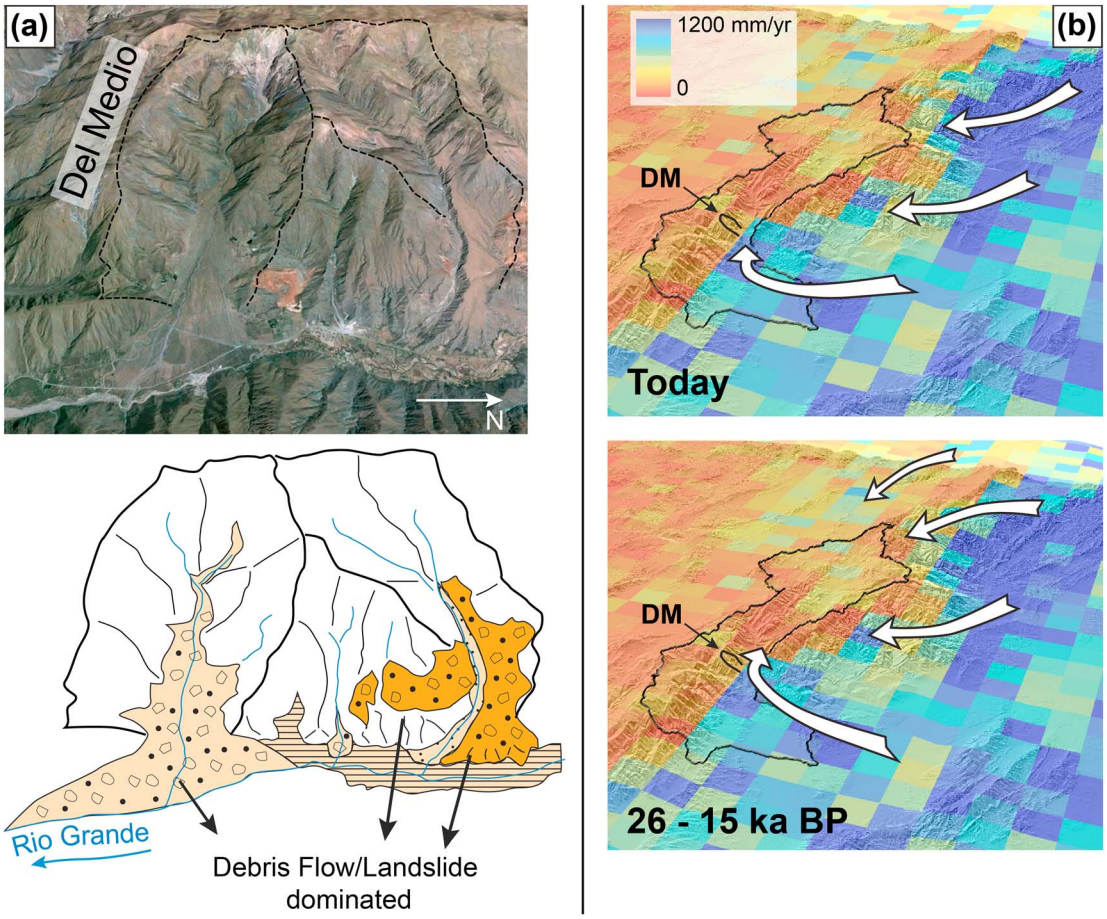

Figure 10. (a) Photograph (upper) and Cartoon (lower) illustrating the similarities between the Del Medio catchment and upstream late Pleistocene fluvial fill terraces. Both the Del Medio fan and the fluvial terraces are formed through debris-flow and landslide processes, implying a northward shift of wetter climatic conditions during the late Pleistocene. (b) Sketches of modern and possible paleo-air-circulations show that in the past a different wind pattern could have brought more moisture into the Humahuaca Basin.

fan, arid conditions may be the reason for the present-day lack of aggradation in the northern catchments due to limited mobilization of sediment on the hillslopes (limited discharge, thus setting transport-limited conditions), despite their steep slopes. Basin-mean erosion rates across the southern Central Andes corroborate this hypothesis, as slower erosion rates (i.e., lower hillslope sediment supply) tend to occur in drier areas [*Bookhagen and Strecker*, 2012].

The similarities between the modern deposits of the Del Medio catchment and the late Pleistocene fill terraces to the north [e.g., *Tschilinguirian and Pereyra*, 2001; *Robinson et al*., 2005; *Rivelli and Flores*, 2009; *May and Soler*, 2010] suggest that the Del Medio catchment may be a modern analog for processes that occurred upstream in the Humahuaca Basin in the past. First, like in the Del Medio catchment, mass movements and debris flows have been suggested to play a major role in the aggradation of the upstream fill terraces (Figure 10a), based on sedimentologic analyses [*May and Soler*, 2010], cosmogenic nuclide-derived denudation rates and grain-size dependencies [*Schildgen et al*., 2016], and stratigraphic-geomorphic relationships farther north [*Tschilinguirian and Pereyra*, 2001; *Strecker et al*., 2007; *Streit et al*., 2015]. Also, the work by *Schildgen et al*. [2016] highlighted the apparent link between a change in climate (particularly a change to wetter conditions) with sediment aggradation. Our hypothesis that aggradation is intimately related to a climatic transition zone is compatible with this notion, considering that just a slight change in the position of that sharp climatic gradient would result in substantially different climatic conditions. Indeed, we might infer that during sediment aggradation in the upper part of the Humahuaca Basin (>40 ka B.P.), the transition between humid and arid sectors was located farther to the north. Studies of modern and paleo-atmospheric circulation patterns have demonstrated that variations in the strength of the SALLJ (South American Low

Level Jet), the CLLJ (Chaco Low Level Jet), and the SACZ (South Atlantic Convergence Zone) through time, which are at least partly linked to Atlantic sea surface temperatures [*Barros et al*., 2000], can lead to enhanced precipitation along the eastern side of the Eastern Cordillera [*Barros et al*., 2000; *Haselton et al*., 2002; *Godfrey et al*., 2003; *Cook and Vizy*, 2006; *Boers et al*., 2013, 2015] (Figure 10b). As such, periods of overall enhanced rainfall may have been associated with farther northward penetration of moisture-bearing air masses from the southern outlet of the Humahuaca Basin, as well as additional rainfall across the relatively low topographic divides to the north (Figure 10b). Although this hypothesis may explain the shift in the locus of aggradation within the Humahuaca Basin through time, more detailed information on the paleo-climatic conditions is needed to verify the link between climatic changes and the onset of aggradation in this area of Argentina.

6. Conclusions

Our field observations, satellite imagery analysis, and ^{10}Be exposure ages and denudation rates help to elucidate the processes that govern the formation of a large alluvial fan along the eastern slopes of the southern Central Andes. We find that nearly the entire surface of the Del Medio fan at the southern end of the Humahuaca Basin has been active throughout the last 400 years. The position of the Del Medio catchment, at a climatic transition between subhumid and arid conditions, combined with the occurrence of rock types prone to failure by mass wasting, appears to be the major drivers for sediment production (landslides) and transport (debris flows) within the Del Medio catchment. The climatic transition zone likely fosters an imbalance between sediment production and transfer within the Del Medio catchment, which periodically receives enough rainfall to mobilize sediment from hillslopes and transport it in debris flows across the fan surface, but has insufficient runoff to remove all of the sediment from the catchment.

The similarities in morphology and sediment transport processes between the Del Medio fan and the late Pleistocene fills farther north in the Humahuaca Basin may suggest that the conditions that govern aggradation in the Del Medio catchment today are similar to those of the northern catchments in the past. Accordingly, the late Pleistocene fills in the Humahuaca Basin may be best explained by a deeper penetration of moisture-bearing air masses into the intermontane basin during past times that were characterized by overall wetter conditions in the Eastern Cordillera. In conclusion, the surface processes and climatic conditions impacting the Del Medio catchment provide an important set of observations for determining what controls alluvial-fan aggradation today and furnish important insights into how climate variability may modulate surface processes in a climatic transition zone through space and time.

Acknowledgments

Additional data used in this paper can be found in the supporting information file. All the data used in the paper are found in the paper or in the supporting information. We acknowledge the team of S. Binnie that performed the AMS analyses of the cosmogenic samples at the University of Cologne, the constructive discussions with C. Cencetti and F. R. Rivelli, and the help of J. Elortegui Palacios. We also greatly appreciated the constructive reviews of Sebastien Carretier, Dylan Ward, and an anonymous reviewer. This project was supported by the Swiss National Science Foundation awarded to S. Savi (Projects PBBEP2_146196 and P300P2_151344), by an Emmy-Noether grant of the German Research Foundation (DFG) awarded to T. Schildgen (grant SCHI 1241/1-1), and DFG grant STR373/32-1 awarded to M. Strecker. Supporting data are included as text, five figures, and seven tables in the associated supporting information file.

References

Acarette du Biscay (1663), Relación de un viaje al Rio de la Plata y de allí por tierra al Perú Con observaciones sobre los habitantes, sean indios o españoles, las ciudades, el comercio, la fertilidad y las riquezas de esta parte de América, trad. Francisco Fernández Wallace y pról. Julio César González, Buenos Aires, Alfer & Vays, 132.

Aguilar, G., S. Carretier, V. Regard, R. Vassallo, R. Riquelme, and J. Martinod (2014), Grain size-dependent ^{10}Be concentrations in alluvial stream sediment of the Huasco Valley, a semi-arid Andes region, *Quat. Geochronol.*, *19*, 163–172, doi:10.1016/j.quageo.2013.01.011.

Analytical Methods Committee (1987), Recommendations for the definition, estimation and use of the detection limit Analyst, February 1987, 112.

Anderson, R. S., J. L. Repka, and G. S. Dick (1996), Explicit treatment of inheritance in dating epositional surfaces using in situ ^{10} Be and ^{26} Al, *Geology*, *1*, 47–51.

Antinao, J. L., and J. Gosse (2009), Large rockslides in the Southern Central Andes of Chile (32–34.5°S): Tectonic control and significance for Quaternary landscape evolution, *Geomorphology*, *104*(3–4), 117–133, doi:10.1016/j.geomorph.2008.08.008.

Balco, G., J. O. Stone, N. A. Lifton, and T. J. Dunai (2008), A complete and easily accessible means of calculating surface exposure ages or erosion rates from ^{10}Be and ^{26}Al measurements, *Quat. Geochronol.*, *3*, 174–195.

Barros, V., M. Gonzalez, B. Liebmann, and I. Camilloni (2000), Influence of the South Atlantic convergence zone and South Atlantic sea surface temperature on interannual summer rainfall variability in Southeastern South America, *Theor. Appl. Climatol.*, *67*, 123–133.

Bekaddour, T., F. Schlunegger, H. Vogel, R. Delunel, K. P. Norton, N. Akçar, and P. Kubik (2014), Paleo erosion rates and climate shifts recorded by Quaternary cut-and-fill sequences in the Pisco valley, central Peru, *Earth Planet. Sci. Lett.*, *390*, 103–115, doi:10.1016/j.epsl.2013.12.048.

Belmont, P., F. J. Pazzaglia, and J. C. Gosse (2007), Cosmogenic ^{10}Be as a tracer for hillslope and channel sediment dynamics in the Clearwater River, western Washington State, *Earth Planet. Sci. Lett.*, *264*(1–2), 123–135, doi:10.1016/j.epsl.2007.09.013.

Bierman, P., and E. J. Steig (1996), Estimating rates of denudation using cosmogenic isotope abundances in sediment, *Earth Surf. Processes Landforms*, *21*, 125–139.

Binnie, S., W. M. Phillips, M. A. Summerfield, and L. K. Fifield (2006), Sediment mixing and basin-wide cosmogenic nuclide analysis in rapidly-eroding mountainous environments, *Quat. Geochronol.*, *1*, 4–14.

Blard, P. H., R. Braucher, J. Lave, and D. Bourles (2013), Cosmogenic Be-10 production rate calibrated against He-3 in the high tropical Andes (3800–4900 m, 20–22°S), *Earth Planet. Sci. Lett.*, *382*, 140–149.

Boers, N., and A. Rheinwalt (2014), The South American rainfall dipole: A complex network analysis of extreme events, *Geophys. Res. Lett.*, *41*, 1–9, doi:10.1002/2014GL061829.1.

Boers, N., B. Bookhagen, N. Marwan, J. Kurths, and J. Marengo (2013), Complex networks identify spatial patterns of extreme rainfall events of the South American Monsoon System, *Geophys. Res. Lett.*, *40*, 4386–4392, doi:10.1002/grl.50681.

Boers, N., B. Bookhagen, J. Marengo, N. Marwan, J. S. Von Storch, and J. Kurths (2015), Extreme rainfall of the South American monsoon system: A dataset comparison using complex networks, *J. Clim.*, *28*(3), 1031–1056, doi:10.1175/JCLI-D-14-00340.1.

Bookhagen, B., and M. R. Strecker (2008), Orographic barriers, high-resolution TRMM rainfall, and relief variations along the eastern Andes, *Geophys. Res. Lett.*, *35*, L06403, doi:10.1029/2007GL032011.

Bookhagen, B., and M. R. Strecker (2012), Spatiotemporal trends in erosion rates across a pronounced rainfall gradient: Examples from the southern Central Andes, *Earth Planet. Sci. Lett.*, *327–328*, 97–110.

Bookhagen, B., K. Haselton, and M. H. Trauth (2001), Hydraulic modelling of a Pleistocene Landslide-dammed lake in the Santa Maria basin, NW Argentina, *Palaeogeol. Palaeoclim. Palaeoecol.*, *169*, 113–27.

Bookhagen, B., R. C. Thiede, and M. R. Strecker (2005), Abnormal monsoon years and their control on erosion and sediment flux in the high, arid northwest Himalaya, *Earth Planet. Sci. Lett.*, *231*, 131–146.

Bookhagen, B., D. Fleitmann, K. Nishiizumi, M. R. Strecker, and R. C. Thiede (2006), Holocene monsoonal dynamics and fluvial terrace formation in the northwest Himalaya, India, *Geology*, *34*(7), 601–604, doi:10.1130/G22698.1.

Braucher, R., P. Del Castillo, L. Siame, A. J. Hidy, and D. L. Bourls (2009), Determination of both exposure time and denudation rate from an in situ-produced ^{10}Be depth profile: A mathematical proof of uniqueness. Model sensitivity and applications to natural cases, *Quat. Geochronol.*, *4*(1), 56–67, doi:10.1016/j.quageo.2008.06.001.

Brown, E. T., R. F. Stallard, M. C. Larsen, G. M. Raisbeck, and F. Yiou (1995), Denudation rates determined from the accumulation of in situ-produced ^{10}Be in the luquillo experimental forest, Puerto Rico, *Earth Planet. Sci. Lett.*, *129*(1–4), 193–202, doi:10.1016/0012-821X(94)00249-X.

Bull, W. B. (1991), *Geomorphic Responses to Climate Change*, pp. 326, Oxford Univ. Press, Oxford, U. K.

Carretier, S., et al. (2015), Differences in ^{10}Be concentrations between river sand, gravel and pebbles along the western side of the central Andes, *Quat. Geochronol.*, *27*, 33–51, doi:10.1016/j.quageo.2014.12.002.

Castino, F., B. Bookhagen, and M. R. Strecker (2016), Rainfall variability and trends of the past six decades (1950–2014) in the subtropical NW Argentine Andes, *Clim. Dyn.*, doi:10.1007/s00382-016-3127-2.

Castro, H. (2001), Cambios en las condiciones de riesgo ambiental en un valle andino del Noroeste argentino Meeting of the Latin American Studies Association, Washington DC, September 6-8, 2001, 17.

Cencetti, C., F. R. Rivelli, and P. Tacconi (2004), Le colate detritiche nell'Arroyo del Medio (Provincia di Jujuy, Argentina nordoccidentale) Proc. of "INTERPRAEVENT 2004" (Riva del Garda, Trento, 24–28 maggio 2004), 1(III), 45–56.

Codilean, A. T., P. Bishop, F. M. Stuart, T. B. Hoey, D. Fabel, and S. P. H. T. Freeman (2008), Single-grain cosmogenic 21Ne concentrations in fluvial sediments reveal spatially variable erosion rates, *Geology*, *36*, 159–162, doi:10.1130/g24360a.1.

Codilean, A. T., C. R. Fenton, D. Fabel, P. Bishop, and S. Xu (2014), Discordance between cosmogenic nuclide concentrations in amalgamated sands and individual fluvial pebbles in an arid zone catchment, *Quat. Geochronol.*, *19*, 4173–4180, doi:10.1016/j.quageo.2012.04.007.

Cook, K. H., and E. K. Vizy (2006), South American climate during the Last Glacial Maximum: Delayed onset of the South American monsoon, *J. Geophys. Res.*, *111*, D02110, doi:10.1029/2005JD005980.

Coulthard, T. J., M. G. Macklin, and M. J. Kirkby (2002), A cellular model of Holocene upland river basin and alluvial fan evolution, *Earth Surf. Processes Landforms*, *27*, 269–288.

Daniels, J. M. (2008), Distinguishing allogenic from autogenic causes of bed elevation change in late Quaternary alluvial stratigraphic records, *Geomorphology*, *101*(1–2), 159–171.

Dethier, D. P., and S. L. Reneau (1996), Lacustrine chronology links late Pleistocene climate change and mass movements in northern New Mexico, *Geology*, *24*, 539–542.

Dühnforth, M., R. S. Anderson, D. Ward, and G. M. Stock (2010), Bedrock fracture control of glacial erosion processes and rates, *Geology*, *38*, 423–426.

Godfrey, L. V., T. E. Jordan, T. K. Lowenstein, and R. L. Alonso (2003), Stable isotope constraints on the transport of water to the Andes between 22° and 26°S during the last glacial cycle, *Palaeogeol. Palaeoclim. Palaeoecol.*, *194*, 299–317.

González Díaz, E. F., and L. E. Fauque (1987), Provenencia del material componental del torrente de barro "El Volcán" Quebrada de Humahuaca, Jujuy – Repubica Argentina Decimo congreso geologico argentino, San Miguel de Tucuman, Actas III, 309–312.

González Díaz, E. F., and R. Mon (2000), El origen de las lagunas de Yala, Provincia de Jujuy (241050 de Latitud Sur y 651280 de Longitud Oeste), in *Actas IV de XIII Congreso Geologico Argentino y III Congreso de Exploracion de Hidrocarburos*, pp. 209–217, Buenos Aires: Asociación Geológica Argentina.

González, M. A., et al. (2000), Ciudad Libertador General San Martín Sheet 2366-IV, scale 1:250000; National Geological Maps of the Argentinean Republic.

Granger, D. E., J. W. Kirchner, and R. Finkel (1996), Spatially averaged long-term erosion rates measured from in situ-produced cosmogenic nuclides in alluvial sediment, *J. Geol.*, *104*(3), 249–257.

Harrington, H. J. (1946), Las corrientes de barro (mud flow) de "El Volcàn", Quebrada de Humahuaca, Jujuy Rev. Asoc. Geologica Argentina, Tomo 1, 2.

Haselton, K., G. Hilley, and M. R. Strecker (2002), Average Pleistocene climatic patterns in the southern central Andes: Controls on mountain glaciation and paleoclimate implications, *J. Geol.*, *110*, 211–226.

Heyman, J., A. P. Stroeven, J. M. Harbor, and M. W. Caffee (2011), Too young or too old: Evaluating cosmogenic exposure dating based on an analysis of compiled boulder exposure ages, *Earth Planet. Sci. Lett.*, *302*, 71–80.

Hidy, A. J., J. C. Gosse, J. L. Pederson, J. P. Mattern, and R. C. Finkel (2010), A geologically constrained Monte Carlo approach to modeling exposure ages from profiles of cosmogenic nuclides: An example from Lees Ferry, Arizona, *Geochem. Geophys. Geosyst.*, *11*, Q0AA10, doi:10.1029/2010GC003084.

Hilley, G. E., and M. R. Strecker (2005), Processes of oscillatory basin filling and excavation in a tectonically active orogen: Quebrada del Toro Basin, NW Argentina, *Bull. Geol. Soc. Am.*, *117*(7–8), 887–901, doi:10.1130/B25602.1.

Istanbulluoglu, E., and R. L. Bras (2006), On the dynamics of soil moisture, vegetation, and erosion: Implications of climate variability and change, *Water Resour. Res.*, *42*, W06418, doi:10.1029/2005WR004113.

Ivy-Ochs, S., and F. Kober (2008), Surface exposure dating with cosmogenic nuclides. Eiszeitalter und Gegenwart, *Quat. Sci. J.*, *57*(1–2), 179–209.

Jezek, P., A. P. Willner, F. G. Acenolaza, and H. Miller (1985), The Puncoviscana trough a large basin of Late Precambrian to Early Cambrian age on the Pacific edge of the Brazilian shield, *Geol. Rundsch.*, *74*, 573–584.
Kirby, E., and K. X. Whipple (2012), Expression of active tectonics in erosional landscapes, *J. Struct. Geol.*, *44*, 54–75, doi:10.1016/j.jsg.2012.07.009.
Kober, F., K. Hippe, B. Salcher, S. Ivy-Ochs, P. W. Kubik, L. Wacker, and N. Hählen (2012), Debris-flow-dependent variation of cosmogenically derived catchment-wide denudation rates, *Geology*, doi:10.1130/G33406.1.
Kohl, C. P., and K. Nishiizumi (1992), Chemical isolation of quartz for measurements of in-situ-produced cosmogenic nuclides, *Geochim. Cosmochim. Acta*, *56*, 3583–3587.
Lal, D. (1991), Cosmic ray labeling of erosion surfaces: In situ nuclide production rates and erosion models, *Earth Planet. Sci. Lett.*, *104*, 424–439.
Lavé, J., and D. Burbank (2004), Denudation processes and rates in the Transverse Ranges, southern California: Erosional response of a transitional landscape to external and anthropogenic forcing, *J. Geophys. Res.*, *109*, F01006, doi:10.1029/2003JF000023.
Lukens, C. E., C. S. Riebe, L. S. Sklar, and D. L. Shuster (2016), Grain size bias in cosmogenic nuclide studies of stream sediment in steep terrain, *J. Geophys. Res. Earth Surf.*, *121*, 978–999, doi:10.1002/2016JF003859.
Lupo, L. C., M. M. Bianchi, E. Araoz, R. Grau, C. Lucas, R. Kern, M. Camacho, W. Tanner, and M. Grosjean (2006), Climate and human impact during the past 2000 years as recorded in the Lagunas de Yala, Jujuy, northwestern Argentina, *Quat. Int.*, *158*, 30–43.
Marcato, G., A. Pasuto, and F. R. Rivelli (2009), Mass movements in the Rio Grande Valley (Quebrada de Humahuaca, Northwestern Argentina): A methodological approach to reduce the risk, *Adv. Geosci.*, *22*, 59–65.
Marengo, J. A., W. R. Soares, C. Saulo, and M. Nicolini (2004), Climatology of the low-level jet east of the Andes as derived from the NCEP-NCAR reanalyses: Characteristics and temporal variability, *J. Clim.*, *17*(12), 2261–2280, doi:10.1175/1520-0442(2004)017<2261:COTLJE>2.0.CO;2.
Margirier, A., L. Audin, J. Carcaillet, S. Schwartz, and C. Benavente (2015), Tectonic and climatic controls on the Chuquibamba landslide (western Andes, southern Peru), *Earth Surf. Dyn.*, *3*(2), 281–289, doi:10.5194/esurf-3-281-2015.
Marrett, R., and M. R. Strecker (2000), Response of intracontinental deformation in the central Andes to late Cenozoic reorganization of South American Plate motions, *Tectonics*, *19*(3), 452–467, doi:10.1029/1999TC001102.
Matmon, A., P. R. Bierman, J. Larsen, S. Southworth, M. Pavich, and M. Caffee (2003), Temporally and spatially uniform rates of erosion in the southern Appalachian Great Smoky Mountains, *Geology*, *31*(2), 155–158, doi:10.1130/0091-7613(2003)031<0155:TASURO>2.0.CO;2.
May, J., and R. D. Soler (2010), Late Quaternary morphodynamics in the Quebrada de Purmamarca, NW Argentina, *Quat. Sci. J.*, *59*(1), 21–35, doi:10.3285/eg.59.1-2.02.
McPhillips, D., P. R. Bierman, T. Crocker, and D. H. Rood (2013), Landscape response to pleistocene-holocene precipitation change in the western cordillera, peru: ^{10}Be concentrations in modern sediments and terrace fills, *J. Geophys. Res. Earth Surf.*, *118*, 2488–2499, doi:10.1002/2013JF002837.
McPhillips, D., P. R. Bierman, and D. H. Rood (2014), Millennial-scale record of landslides in the Andes consistent with earthquake trigger, *Nat. Geosci.*, *7*(12), 925–930, doi:10.1038/ngeo2278.
Mechoso, C. R., A. W. Robertson, C. F. Ropelewski, and A. M. Grimm (2005), The American Monsoon Systems, *Glob. Monsoon Syst. Res. Forecast.*, *13*(2004), 197–206.
Mocak, J., A. M. Bond, S. Mitchell, and G. Scollary (1997), A statistical overview of standard (IUPAC and ACS) and new procedures for determining the limits of detection and quantification: Application to voltammetric and stnpping techniques, *Pure Appl. Chem.*, *69*(2), 297–328.
Montgomery, D. R., and E. Foufoula-Georgiou (1994), Channel network source representation using digital elevation models, *Water Resour. Res.*, *29*(12), 3925–3934, doi:10.1029/93WR02463.
Moreiras, S. M., and A. Coronato (2010), Landslide processes in Argentina, in *Natural Hazards and Human-Exacerbated Disasters in Latin America*, *Dev. Earth Surf. Processes*, vol. 13, pp. 301–332, Elsevier, Oxford.
Niemi, N. A., M. Oskin, D. W. Burbank, A. M. Heimsath, and E. J. Gabet (2005), Effects of bedrock landslides on cosmogenically determined erosion rates, *Earth Planet. Sci. Lett.*, *237*(3–4), 480–498, doi:10.1016/j.epsl.2005.07.009.
Nishiizumi, K., M. Imamura, M. W. Caffee, J. R. Southon, R. C. Finkel, and J. McAninch (2007), Absolute calibration of ^{10}Be AMS standards, *Nucl. Instrum. Methods Phys. Res., Sect. B*, *258*(2), 403–413, doi:10.1016/j.nimb.2007.01.297.
Paolini, L., R. Villalba, and H. R. Grau (2005), Precipitation variability and landslide occurrence in a subtropical mountain ecosystem of NW Argentina, *Dendrochronologia*, *22*(3), 175–180.
Pastore, F. Y., and P. Groeber (1931), *Reconocimiento Geologico del Torrente de Barro Llamado Volcàn, Valle de Humahuaca, Jujuy*, *An. Mus. Nac. Hist. Nat.*, vol. 36, pp. 1–15, Buenos Aires.
Pingel, H., M. R. Strecker, R. N. Alonso, and A. K. Schmitt (2013), Neotectonic basin and landscape evolution in the Eastern Cordillera of NW Argentina, Humahuaca Basin (~24S), *Basin Res.*, *25*(5), 554–573, doi:10.1111/bre.12016.
Pingel, H., R. N. Alonso, A. Mulch, A. Rohrmann, M. Sudo, and M. R. Strecker (2014), Pliocene orographic barrier uplift in the southern Central Andes, *Geology*, *42*(8), 691–694, doi:10.1130/G35538.1.
Rivelli, F. R., and E. M. Flores (2009), *Protección de márgenes en el Río Grande, tramo las Quebradas Trancas – Tilcara*, Cuarto Simposio Regional sobre Hidráulica de Ríos, Salta, Argentina.
Robinson, R. A. J., J. Q. G. Spencer, M. R. Strecker, A. Richter, and R. N. Alonso (2005), Luminescence dating of alluvial fans in intramontane basins of NW Argentina, *Geol. Soc. London, Spec. Publ.*, *251*, 153–168, doi:10.1144/GSL.SP.2005.251.01.11.
Rodríguez Fernández, L. R., N. Heredia, R. E. Seggiaro, and M. González (1999), Estructura andina de la Cordillera Oriental en el _area de la Quebrada de Humahuaca, Provincia de Jujuy, NO de Argentina, *Trab. Geol.*, *21*, 321–332.
Salio, P., M. Nicolini, and A. C. Saulo (2002), Chaco low-level jet events characterization during the austral summer season, *J. Geophys. Res.*, *107*(24), 4816, doi:10.1029/2001JD001315.
Savi, S., K. Norton, V. Picotti, F. Brardinoni, N. Akçar, P. W. Kubik, R. Delunel, and F. Schlunegger (2014), Effects of sediment mixing on ^{10}Be concentrations in the Zielbach catchment, central-eastern Italian Alps, *Quat. Geochronol.*, *19*, 148–162, doi:10.1016/j.quageo.2013.01.006.
Schaller, M., F. von Blanckenburg, A. Veldkamp, L. A. Tebbens, N. Hovius, and P. W. Kubik (2002), 30,000 yr record of erosion rates from cosmogenic ^{10}Be in Middle European river terraces, *Earth Planet. Sci. Lett.*, *204*, 307–320.
Scherler, D., B. Bookhagen, and M. R. Strecker (2014), Tectonic control on 10Be-derived erosion rates in the Garhwal Himalaya, India, *J. Geophys. Res. Earth Surf.*, *119*, 83–105, doi:10.1002/2013JF002955.
Scherler, D., M. P. Lamb, E. J. Rhodes, and J. Avouac (2016), Climate-change versus landslide origin of fill terraces in a rapidly eroding bedrock landscape: San Gabriel River, California, *GSA Bull.*, *128*(7–8), 1228–1248, doi:10.1130/B31356.1.
Schildgen, T. F., D. P. Dethier, P. Bierman, and M. Caffee (2002), ^{26}Al and ^{10}Be dating of late Pleistocene and Holocene fill terraces: A record of fluvial deposition and incision, Colorado Front Range, *Earth Surf. Processes Landforms*, *27*(7), 773–787.

Schildgen, T. F., et al. (2016), Landscape response to late Pleistocene climate change in NW Argentina: Sediment flux modulated by basin geometry and connectivity, *J. Geophys. Res. Earth Surf.*, *121*, 392–414, doi:10.1002/2015JF003607.

Schumm, S. A., and R. S. Parker (1973), Implications of complex response of drainage systems for Quaternary alluvial stratigraphy, *Nat. (Phys. Sci.)*, *243*, 110–119.

Schwanghart, W., and D. Scherler (2014), Short Communication: TopoToolbox 2—MATLAB-based software for topographic analysis and modeling in Earth surface sciences, *Earth Surf. Dyn.*, *2*(1), 1–7, doi:10.5194/esurf-2-1-2014.

Siame, L., et al. (2004), Local erosion rates versus active tectonics: Cosmic ray exposure modelling in Provence (south-east France), *Earth Planet. Sci. Lett.*, *220*(3–4), 345–364, doi:10.1016/S0012-821X(04)00061-5.

Silva, V. B. S., and V. E. Kousky (2012), The South American Monsoon System: Climatology and variability, *Mod. Climatol.*, *398*.

Slingerland, R. L., and R. S. Snow (1988), Stability analysis of a rejuvenated fluvial system, *Z. Geomorphol.*, *67*, 93–102.

Steffen, D., F. Schlunegger, and F. Preusser (2009), Drainage basin response to climate change in the Pisco valley, *Peru Geol.*, *37*(6), 491–494, doi:10.1130/G25475A.1.

Steffen, D., F. Schlunegger, and F. Preusser (2010), Late Pleistocene fans and terraces in the Majes valley, southern Peru, and their relation to climatic variations, *Int. J. Earth Sci.*, *99*(8), 1975–1989, doi:10.1007/s00531-009-0489-2.

Stock, J. D., and W. E. Dietrich (2003), Valley incision by debris flows: Evidence of a topographic signature, *Water Resour. Res.*, *39*(4), 1089–1113, doi:10.1029/2001WR001057.

Stock, J. D., and W. E. Dietrich (2006), Erosion of steepland valleys by debris flows, *Bull. Geol. Soc. Am.*, *118*(9–10), 1125–1148, doi:10.1130/B25902.1.

Stone, J. O. (2000), Air pressure and cosmogenic isotope production, *J. Geophys. Res.*, *105*(B10), 23,753–23,759, doi:10.1029/2000JB900181.

Strecker, M. R., R. N. Alonso, B. Bookhagen, B. Carrapa, G. E. Hilley, E. R. Sobel, and M. H. Trauth (2007), Tectonics and climate of the Southern Central Andes, *Annu. Rev. Earth Planet. Sci.*, *35*, 747–87.

Streit, R. L., D. W. Burbank, M. R. Strecker, R. N. Alonso, J. M. Cottle, and A. R. C. Kylander-Clark (2015), Controls on intermontane basin filling, isolation and incision on themargin of the Puna Plateau,NW Argentina (~23°S), *Basin Res.*, 1–25, doi:10.1111/bre.12141.

Torres-Acosta, V., T. F. Schildgen, B. A. Clarke, D. Scherler, B. Bookhagen, H. Wittmann, W. Ouimet, F. von Blanckenburg, and M. R. Strecker (2015), The effect of vegetation cover on millenial-scale landscape denudation in East Africa, *Lithosphere*, *7*, 408–420.

Trauth, M. H., R. A. Alonso, K. R. Haselton, R. L. Hermanns, and M. R. Strecker (2000), Climate change and mass movements in the NW Argentine Andes, *Earth Planet. Sci. Lett.*, *179*(2), 243–256, doi:10.1016/S0012-821X(00)00127-8.

Trauth, M. H., B. Bookhagen, N. Marwan, and M. R. Strecker (2003), Multiple landslide clusters record Quaternary climate changes in the northwestern Argentine Andes, *Palaeogeogr. Palaeoclimatol. Palaeoecol.*, *194*(1-3), 109–121, doi:10.1016/S0031-0182(03)00273-6.

Tschilinguirian, P., and F. X. Pereyra (2001), Geomorfología del sector Salinas Grandes- Quebrada de Humahuaca, provincia de Jujuy, *Rev. Asoc. Geol. Argent.*, *56*(1), 3–15.

Vera, C., et al. (2006), The South American low-level jet experiment, *Bull. Am. Meteorol. Soc.*, *87*(1), 63–77, doi:10.1175/BAMS-87-1-63.

von Blanckenburg, F. (2004), Cosmogenic nuclide evidence for low weathering and denudation in the wet, tropical highlands of Sri Lanka, *J. Geophys. Res.*, *109*, F03008, doi:10.1029/2003JF000049.

von Blanckenburg, F. (2005), The control mechanisms of erosion and weathering at basin scale from cosmogenic nuclides in river sediment, *Earth Planet. Sci. Lett.*, *237*(3–4), 462–479, doi:10.1016/j.epsl.2005.06.030.

Weigert, R. S. G., S. A. Chalabe, and L. E. Maigua (2010), Efectos de la intervención humana en la dinámica erosiva del río Grande de Jujuy entre Volcán-"Peña Azul" (departamento Tumbaya, provincia de Jujuy) VI Jornadas de Ciencia y Tecnología de las Facultades de Ingeniería del NOA Publicación: Investigaciones en Facultades de Ingeniería del NOA-2010; Págs. 243–247.

Weiss, A. D. (2001), Topographic Position and Landforms Analysis Poster at 21st ESRI Int'l User Conference.

Whipple, K. X. (2004), Bedrock rivers and the geomorphology of active orogens, *Annu. Rev. Earth Planet. Sci.*, *32*, 151–85, doi:10.1146/annurev.earth.32.101802.120356.

Yanites, B. J., G. E. Tucker, and R. S. Anderson (2009), Numerical and analytical models of cosmogenic radionuclide dynamics in landslide-dominated drainage basins, *J. Geophys. Res.*, *114*, F01007, doi:10.1029/2008JF001088.